



Universiteit
Leiden
The Netherlands

Tailoring x-ray tomography techniques for cultural heritage research

Bossema, F.G.

Citation

Bossema, F. G. (2024, May 23). *Tailoring x-ray tomography techniques for cultural heritage research*. Retrieved from <https://hdl.handle.net/1887/3754491>

Version: Publisher's Version

[Licence agreement concerning inclusion of doctoral thesis in the Institutional Repository of the University of Leiden](#)

License: <https://hdl.handle.net/1887/3754491>

Note: To cite this publication please use the final published version (if applicable).

Bibliography

- [1] W. V. Aarle, W. J. Palenstijn, J. Cant, E. Janssens, F. Bleichrodt, A. Dabravolski, J. D. Beenhouwer, K. J. Batenburg, and J. Sijbers. “Fast and flexible X-ray tomography using the ASTRA toolbox”. *Optics Express* 24.22 (2016), pp. 25129–25147 (cit. on pp. 50, 70).
- [2] M. Abella, C. Martinez, I. Garcia, P. Moreno, C. De Molina, and M. Desco. “Tolerance to geometrical inaccuracies in CBCT systems: A comprehensive study”. *Medical Physics* 48.10 (Oct. 2021), pp. 6007–6019 (cit. on p. 69).
- [3] A. Adriaens. “Non-destructive analysis and testing of museum objects: An overview of 5 years of research”. *Spectrochimica Acta - Part B Atomic Spectroscopy* 60.12 (2005), pp. 1503–1516 (cit. on p. 41).
- [4] F. Albertin, M. Bettuzzi, R. Brancaccio, M. P. Morigi, and F. Casali. “X-Ray Computed Tomography In Situ: An Opportunity for Museums and Restoration Laboratories”. *Heritage* 2.3 (2019), pp. 2028–2038 (cit. on pp. 27, 60).
- [5] J. Anderson and D. Antoine. “Scanning Sobek, Mummy of the Crocodile God”. In: *Creatures of Earth, Water and Sky: Essays on Animals in Ancient Egypt and Nubia*. Leiden: Sidestone Press, 2019, pp. 31–37 (cit. on pp. 23, 24).
- [6] F. I. Apollonio, F. Fantini, S. Garagnani, and M. Gaiani. “A Photogrammetry-Based Workflow for the Accurate 3D Construction and Visualization of Museums Assets”. *Remote Sensing* 13.3 (2021), p. 486 (cit. on p. 77).
- [7] ARES. *Astromaterials 3D*. URL: <https://ares.jsc.nasa.gov/astromaterials3d/> (visited on Nov. 9, 2023) (cit. on pp. 78, 79).
- [8] Artec 3D. *Egyptian mummy turned into 3D model*. 2017. URL: <https://www.artec3d.com/news/computed-tomography-3d-scanning-egyptian-mummy> (visited on Nov. 9, 2023) (cit. on p. 79).
- [9] Autodesk. *Maya Software*. URL: <https://www.autodesk.eu/products/maya/overview> (visited on Nov. 9, 2023) (cit. on p. 78).
- [10] Autograd. URL: <https://github.com/HIPS/autograd> (visited on Nov. 9, 2023) (cit. on p. 127).
- [11] Avrotros. *Historisch Bewijs - De boekenkist van Hugo de Groot*. URL: <https://www.avrotros.nl/archive/historisch-bewijs-de-boekenkist-van-hugo-de-groot-04-03-2020~osixpw0e/> (visited on Nov. 9, 2023) (cit. on pp. 52, 100).
- [12] M. G. L. Baillie. *Tree-ring dating and archaeology*. Vol. 3. 1982 (cit. on pp. 42, 47).
- [13] M. G. L. Baillie and J. R. Pilcher. “A simple crossdating program for tree-ring research”. *Tree-Ring Bulletin* 33 (1973), pp. 7–14 (cit. on pp. 47, 49, 52).

- [14] F. Bauer, D. Forndran, T. Schromm, and C. U. Grosse. "Practical Part-Specific Trajectory Optimization for Robot-Guided Inspection via Computed Tomography". *Journal of Nondestructive Evaluation* 41.3 (2022), p. 55 (cit. on p. 69).
- [15] L. Beck. "Recent trends in IBA for cultural heritage studies". *Nuclear Instruments and Methods in Physics Research, Section B: Beam Interactions with Materials and Atoms* 332 (2014). Publisher: Elsevier, pp. 439–444 (cit. on p. 41).
- [16] G. Bekes, E. Máté, L. G. Nyúl, A. Kuba, and M. Fidrich. "Geometrical model-based segmentation of the organs of sight on CT images: Geometrical model-based segmentation of the organs of sight". *Medical Physics* 35.2 (2008), pp. 735–743 (cit. on pp. 5, 24).
- [17] L. Bertrand, S. Schöeder, D. Anglos, M. B. Breese, K. Janssens, M. Moini, and A. Simon. "Mitigation strategies for radiation damage in the analysis of ancient materials". *TrAC Trends in Analytical Chemistry* 66 (2015), pp. 128–145 (cit. on pp. 26, 101).
- [18] M. Bettuzzi, F. Casali, M. P. Morigi, R. Brancaccio, D. Carson, G. Chiari, and J. Maish. "Computed tomography of a medium size Roman bronze statue of Cupid". *Applied Physics A* 118.4 (2015), pp. 1161–1169 (cit. on pp. 26, 60).
- [19] J. Bill, A. Daly, Ø. Johnsen, and K. S. Dalen. "DendroCT - Dendrochronology without damage". *Dendrochronologia* 30.3 (2012), pp. 223–230 (cit. on pp. 12, 24, 42, 69).
- [20] Blender Foundation. *blender.org - Home of the Blender project*. URL: <https://www.blender.org/> (visited on Nov. 9, 2023) (cit. on p. 78).
- [21] F. E. Boas and D. Fleischmann. "CT artifacts: causes and reduction techniques". *Imaging in Medicine* 4.2 (2012), pp. 229–240 (cit. on p. 26).
- [22] F. Bossema. *Code for 3D tomography using only basic X-ray equipment and metal markers*. 2024. URL: <https://zenodo.org/records/8379920> (visited on Mar. 19, 2024) (cit. on pp. 61, 150).
- [23] F. Bossema. *Radiographic data of a wooden block with metal markers at the Flex-ray laboratory (high resolution)*. 2024. URL: <https://zenodo.org/records/10557034> (visited on Mar. 19, 2024) (cit. on pp. 63, 150).
- [24] F. Bossema. *Radiographic data of a wooden block with metal markers at the Rijksmuseum X-ray facility*. 2024. URL: <https://zenodo.org/records/8379870> (visited on Mar. 19, 2024) (cit. on pp. 63, 150).
- [25] F. Bossema and A. Heginbotham. *Radiographic data of a wooden block with metal markers at the J. Paul Getty Museum X-ray facility*. 2024. URL: <https://zenodo.org/records/8379880> (visited on Mar. 19, 2024) (cit. on pp. 63, 150).
- [26] F. Bossema, A. Heginbotham, and M. Corona. *Radiographic data of 'Python killing a Gnu' by Antoine-Louis Barye, The J. Paul Getty Museum collection*. 2024. URL: <https://zenodo.org/records/8379913> (visited on Mar. 19, 2024) (cit. on pp. 66, 150).

- [27] F. Bossema and D. O'Flynn. *Radiographic data of a wooden block with metal markers at the British Museum X-ray facility*. 2024. URL: <https://zenodo.org/records/8379910> (visited on Mar. 19, 2024) (cit. on pp. 63, 150).
- [28] F. Bossema, J. Retrê, S. Pereira, and P. Russo. "Your night out under the stars: Reaching beyond native audiences". *Communicating Astronomy with the Public* (2018) (cit. on p. 150).
- [29] F. Bossema and P. Van Laar. *CT reconstruction and structured light scan of a small wooden block*. 2023. URL: <https://zenodo.org/records/8041816> (visited on Nov. 9, 2023) (cit. on p. 151).
- [30] F. Bossema, P. Van Laar, and K. Meechan. *IntACT plugin for Blender*. 2023. URL: <https://zenodo.org/records/8041844> (visited on Nov. 9, 2023) (cit. on p. 151).
- [31] F. Bossema, C. Zwetsloot, and I. Smeets. "Math in the City: Designing a Math Trail for High School Students". In: *World Scientific Series on Science Communication*. Vol. 03. WORLD SCIENTIFIC, 2023, pp. 53–72 (cit. on p. 149).
- [32] F. G. Bossema. *A CT dataset of a small wooden block*. 2021. URL: <https://zenodo.org/record/4533882> (visited on Nov. 9, 2023) (cit. on pp. 48, 151).
- [33] F. G. Bossema. *A line trajectory X-ray tomography dataset of a wooden plank*. 2021. URL: <https://zenodo.org/record/4533887> (visited on Nov. 9, 2023) (cit. on pp. 51, 151).
- [34] F. G. Bossema. *Three line trajectory X-ray tomography datasets of a small wooden block*. 2021. URL: <https://zenodo.org/record/4541555> (visited on Nov. 9, 2023) (cit. on pp. 48, 151).
- [35] F. G. Bossema, P. Burger, L. Bratton, A. Challenger, R. C. Adams, P. Sumner, J. Schat, M. E. Numans, and I. Smeets. "Expert quotes and exaggeration in health news: a retrospective quantitative content analysis". *Wellcome Open Research* 4 (2019), p. 56 (cit. on p. 150).
- [36] F. G. Bossema and S. B. Coban. *Three tomographic CT datasets of a woven fabric*. 2020. URL: <https://zenodo.org/records/3741311> (visited on Nov. 9, 2023) (cit. on pp. 28, 151).
- [37] F. G. Bossema, S. B. Coban, A. Kostenko, P. van Duin, J. Dorscheid, I. Garachon, E. Hermens, R. van Liere, and K. J. Batenburg. "Integrating expert feedback on the spot in a time-efficient explorative CT scanning workflow for cultural heritage objects". *Journal of Cultural Heritage* 49 (2021), pp. 38–47 (cit. on pp. 23, 41, 60, 70, 78, 90, 149).
- [38] F. G. Bossema, M. Domínguez-Delmás, W. J. Palenstijn, A. Kostenko, J. Dorscheid, S. B. Coban, E. Hermens, and K. J. Batenburg. "A novel method for dendrochronology of large historical wooden objects using line trajectory X-ray tomography". *Scientific Reports* 11, 11024 (2021) (cit. on pp. 41, 69, 149).

- [39] F. G. Bossema, J. Dorscheid, A. Kostenko, and S. B. Coban. *A line trajectory X-ray tomography dataset of the Hugo de Groot bookchest*. 2021. URL: <http://zenodo.org/record/4533923> (visited on Nov. 9, 2023) (cit. on pp. 53, 151).
- [40] F. G. Bossema, A. Kostenko, and S. B. Coban. *A five-tile tomographic micro-CT dataset of the oak sculpture "Holy woman with lantern" - part 1 of 2*. 2020. URL: <https://zenodo.org/record/3747192> (visited on Nov. 9, 2023) (cit. on pp. 30, 151).
- [41] F. G. Bossema, A. Kostenko, and S. B. Coban. *A five-tile tomographic micro-CT dataset of the oak sculpture "Holy woman with lantern" - part 2 of 2*. 2020. URL: <https://zenodo.org/record/3747327> (visited on Nov. 9, 2023) (cit. on pp. 30, 151).
- [42] F. G. Bossema, W. J. Palenstijn, A. Heginbotham, M. Corona, T. Van Leeuwen, R. Van Liere, J. Dorscheid, D. O'Flynn, J. Dyer, E. Hermens, and K. J. Batenburg. "Enabling 3D CT-scanning of cultural heritage objects using only in-house 2D X-ray equipment in museums". *Nature Communications* (accepted, in press) (cit. on pp. 59, 121, 149).
- [43] F. G. Bossema, P. J. Van Laar, K. Meechan, D. O'Flynn, J. Dyer, T. Van Leeuwen, S. Meijer, E. Hermens, and K. J. Batenburg. "Inside out: Fusing 3D imaging modalities for the internal and external investigation of multi-material museum objects". *Digital Applications in Archaeology and Cultural Heritage* 31 (2023), e00296 (cit. on pp. 77, 84, 86, 133, 149).
- [44] R. Brancaccio, M. Bettuzzi, F. Casali, M. P. Morigi, G. Levi, A. Gallo, G. Marchetti, and D. Schneberk. "Real-time reconstruction for 3-D CT applied to large objects of cultural heritage". *IEEE Transactions on Nuclear Science* 58.4 (2011), pp. 1864–1871 (cit. on pp. 42, 55).
- [45] British Museum - *Scientific techniques*. URL: <https://www.britishmuseum.org/our-work/departments/scientific-research/scientific-techniques> (visited on Nov. 9, 2023) (cit. on p. 55).
- [46] M. Brookhouse, S. Ives, P. Dredge, D. Howard, and M. Bridge. "Mapping Henry: Dendrochronological Analysis of a Sixteenth-Century Panel Painting Based Upon Synchrotron-Sourced X-ray Fluorescence Mapping". *Studies in Conservation* (2020), pp. 1–13 (cit. on p. 41).
- [47] J. V. d. Bulcke, D. V. Loo, M. Dierick, B. Masschaele, L. V. Hoorebeke, and J. V. Acker. "Nondestructive research on wooden musical instruments: From macro- to microscale imaging with lab-based X-ray CT systems". *Journal of Cultural Heritage* 27.Supplement (2017), S78–S87 (cit. on pp. 13, 24, 26, 42).
- [48] T. Buzug. *Computed tomography: From photon statistics to modern cone-beam CT*. Springer-Verlag Berlin Heidelberg, 2008 (cit. on pp. 6, 24, 26, 44, 72).
- [49] M. Carl and M. L. Young. "Complementary analytical methods for analysis of Ag-plated cultural heritage objects". *Microchemical Journal* 126 (2016). Publisher: Elsevier Inc., pp. 307–315 (cit. on p. 41).

- [50] F. Casali. “Chapter 2 X-ray and neutron digital radiography and computed tomography for cultural heritage”. In: *Physical Techniques in the Study of Art, Archaeology and Cultural Heritage*. Vol. 1. Elsevier, 2006, pp. 41–123 (cit. on pp. 6, 24, 26).
- [51] Centrum Wiskunde & Informatica. *NWO Team Science Award for CWI with UvA and Rijksmuseum*. URL: <https://www.cwi.nl/en/news/nwo-team-science-award-for-cwi-and-research-partners/> (visited on Nov. 9, 2023) (cit. on p. 100).
- [52] P. Cignoni, M. Callieri, M. Corsini, M. Dellepiane, F. Ganovelli, and G. Ranzuglia. “MeshLab: an Open-Source Mesh Processing Tool”. In: *Eurographics Italian Chapter Conference*. Ed. by V. Scarano, R. D. Chiara, and U. Erra. The Eurographics Association, 2008 (cit. on p. 78).
- [53] S. B. Coban, F. Lucka, W. J. Palenstijn, D. Van Loo, and K. J. Batenburg. “Explorative Imaging and Its Implementation at the FleX-ray Laboratory”. *Journal of Imaging* 6.4 (2020), p. 18 (cit. on pp. 27, 46, 86).
- [54] A. Netherlands Institute for Conservation and Science. *CT for Art*. URL: <https://www.nicas-research.nl/projects/impact4art/> (visited on Nov. 9, 2023) (cit. on p. 25).
- [55] B. Cornelis, T. Ruxzić, E. Gezels, A. Dooms, A. Pixzurica, L. Platiixa, J. Cornelis, M. Martens, M. De Mey, and I. Daubechies. “Crack detection and inpainting for virtual restoration of paintings: The case of the Ghent Altarpiece”. *Signal Processing* 93.3 (2013), pp. 605–619 (cit. on p. 23).
- [56] B. Cornelis, A. Dooms, I. Daubechies, and P. Schelkens. “Report on Digital Image Processing for Art Historians”. In: *SAMPTA ’09, Marseille, France. Special session on sampling and (in)painting*. 2009 (cit. on pp. 23, 41).
- [57] I. Dakir. *BDENTAL*. 2022. URL: <https://github.com/issamdakir/BDENTAL> (visited on Nov. 9, 2023) (cit. on p. 83).
- [58] A. Daly and N. L. W. Streeton. “Non-invasive dendrochronology of late-medieval objects in Oslo: refinement of a technique and discoveries”. *Applied Physics A* 123.6 (2017), p. 431 (cit. on pp. 12, 24, 42, 60).
- [59] J. Dambrøg, A. Ghassaei, D. S. Smith, H. Jackson, M. L. Demaine, G. Davis, D. Mills, R. Ahrendt, N. Akkerman, D. van der Linden, and E. D. Demaine. “Unlocking history through automated virtual unfolding of sealed documents imaged by X-ray microtomography”. *Nature Communications* 12.1 (2021). Number: 1 Publisher: Nature Publishing Group, p. 1184 (cit. on pp. 59, 60, 101).
- [60] M. Domínguez-Delmás, F. G. Bossema, J. Dorscheid, M. Hall-Aquitania, S. B. Coban, K. J. Batenburg, and E. Hermens. “X-ray computed tomography for non-invasive dendrochronology reveals concealed double paneling on a painting from Rubens’ studio”. *PLOS ONE* (2021) (cit. on pp. 11, 60, 100, 150).

- [61] M. Domínguez-Delmás, P. Van Duin, J. Dorscheid, F. G. Bossema, K. J. Batenburg, and R. Van Langh. “Unravelling a 17th-century prison escape: The quest to identify the original Hugo Grotius bookchest”. In: *Working Towards a Sustainable Past*. ICOM-CC 20th Triennial Conference Preprints, Valencia, 18–22 September 2023, J. Bridgland. Paris: International Council of Museums, 2023 (cit. on pp. 100, 149).
- [62] M. Domínguez-Delmás. “Seeing the forest for the trees: New approaches and challenges for dendroarchaeology in the 21st century”. *Dendrochronologia* 62.October 2019 (2020). Publisher: Elsevier, p. 125731 (cit. on pp. 41, 42).
- [63] M. Domínguez-Delmás, F. G. Bossema, B. van der Mark, A. Kostenko, S. B. Coban, S. van Daalen, P. van Duin, and K. J. Batenburg. “Dating and provenancing the Woman with lantern sculpture – A contribution towards attribution of Netherlandish art”. *Journal of Cultural Heritage* 50 (2021), pp. 179–187 (cit. on pp. 3, 12, 23, 30, 59, 60, 100, 150).
- [64] J. Dorscheid, F. G. Bossema, P. van Duin, S. B. Coban, R. van Liere, K. J. Batenburg, and G. P. Di Stefano. “Looking under the skin: multi-scale CT scanning of a peculiarly constructed cornett in the Rijksmuseum”. *Heritage Science* 10, 161.1 (2022) (cit. on pp. 38, 59, 78, 100, 149).
- [65] A. Douglass. “Crossdating in Dendrochronology”. *Journal of Forestry* 39.10 (1941) (cit. on p. 42).
- [66] *Dragonfly*. URL: <https://www.theobjects.com/dragonfly/index.html> (visited on Nov. 9, 2023) (cit. on pp. 11, 79).
- [67] Dutch Research Council (NWO). *Winners NWO Science Awards 2021 announced*. URL: <https://www.nwo.nl/en/news/winners-nwo-science-awards-2021-announced> (visited on Nov. 9, 2023) (cit. on p. 100).
- [68] D. Eckstein and J. Bauch. “Beitrag zur Rationalisierung eines dendrochronologischen Verfahrens und zu Analyse seiner Aussagesicherheit”. *Forstwissenschaftliches Centralblatt* 88 (1969), pp. 230–250 (cit. on pp. 47, 49, 52).
- [69] *Ethafoam - CAMEO*. URL: <https://cameo.mfa.org/wiki/Ethafoam> (visited on Nov. 9, 2023) (cit. on p. 33).
- [70] S. Fahrni, L. Campana, A. Dominguez, T. Uldin, F. Dedouit, O. Delémont, and S. Grabherr. “CT-scan vs. 3D surface scanning of a skull: first considerations regarding reproducibility issues”. *Forensic sciences research* 2.2 (2017), pp. 93–99 (cit. on p. 79).
- [71] A. Fedorov, R. Beichel, J. Kalpathy-Cramer, J. Finet, J.-C. Fillion-Robin, S. Pujol, C. Bauer, D. Jennings, F. Fennessy, M. Sonka, J. Buatti, S. Aylward, J. V. Miller, S. Pieper, and R. Kikinis. “3D Slicer as an image computing platform for the Quantitative Imaging Network”. *Magnetic Resonance Imaging* 30.9 (2012), pp. 1323–1341 (cit. on pp. 11, 79).
- [72] L. A. Feldkamp, L. C. Davis, and J. W. Kress. “Practical cone-beam algorithm”. *Journal of the Optical Society of America A* 1.6 (1984), pp. 612–619 (cit. on pp. 9, 44, 71).

- [73] M. Ferrucci, R. K. Leach, C. Giusca, S. Carmignato, and W. Dewulf. “Towards geometrical calibration of x-ray computed tomography systems—a review”. *Measurement Science and Technology* 26.9 (Sept. 2015), p. 092003 (cit. on p. 69).
- [74] M Feser, J Gelb, H Chang, H Cui, F Duewer, S. H. Lau, A Tkachuk, and W Yun. “Sub-micron resolution CT for failure analysis and process development”. *Measurement Science and Technology* 19.9 (2008), p. 094001 (cit. on p. 24).
- [75] M. Fioravanti, G. Di Giulio, G. Signorini, G. R. Rognoni, N. Sodini, G. Tromba, and F. Zanini. “Non-invasive wood identification of historical musical bows”. *IAWA Journal* 38.3 (2017), pp. 285–296 (cit. on p. 42).
- [76] P. Fraiture. “Contribution of dendrochronology to understanding of wood procurement sources for panel paintings in the former Southern Netherlands from 1450 AD to 1650 AD”. *Dendrochronologia* 27.2 (2009). Publisher: Elsevier, pp. 95–111 (cit. on p. 51).
- [77] P. Fried, J. Woodward, D. Brown, D. Harvell, and J. Hanken. “3D scanning of antique glass by combining photography and computed tomography”. *Digital Applications in Archaeology and Cultural Heritage* 18 (2020), e00147 (cit. on pp. 23, 59, 78, 79).
- [78] H. C. Fritts. *Tree rings and climate*. Academic Press, London, 1976 (cit. on p. 42).
- [79] H. Gao, L. Zhang, Z. Chen, Y. Xing, J. Cheng, and Z. Qi. “Direct filtered-backprojection-type reconstruction from a straight-line trajectory”. *Optical Engineering* 46.5 (2007), p. 057003 (cit. on p. 43).
- [80] H. Gao, L. Zhang, Z. Chen, Y. Xing, H. Xue, and J. Cheng. “Straight-line-trajectory-based x-ray tomographic imaging for security inspections: System design, image reconstruction and preliminary results”. *IEEE Transactions on Nuclear Science* 60.5 (2013), pp. 3955–3968 (cit. on p. 43).
- [81] I. Garachon. “Some technical aspects of the terracotta models from the estate of Johan Gregor van der Schardt”. *Simiolus Neth. Q. Hist. Art* 41 (2020), pp. 177–190 (cit. on pp. 13, 24, 78).
- [82] I. Garachon and L. Van Valen. “The matter of tang tomb figures: A new perspective on a group of terracotta animals and riders”. *Rijksmuseum Bulletin* (2014), pp. 218–239 (cit. on pp. 23, 24, 26).
- [83] P. Garside and S. O’Connor. “Assessing the risks of radiographing culturally significant textiles”. *e-Preservation science* (2007) (cit. on pp. 26, 101).
- [84] S. Gondrom, J. Zhou, M. Maisl, H. Reiter, M. Kröning, and W. Arnold. “X-ray computed laminography: An approach of computed tomography for applications with limited access”. *Nuclear Engineering and Design* 190 (1999), pp. 141–147 (cit. on p. 43).
- [85] R. C. Gonzalez and R. E. Woods. *Digital Image Processing*. 3rd Editio. Prentice-Hall, 2007 (cit. on p. 53).

- [86] J. Graetz. “Auto-calibration of cone beam geometries from arbitrary rotating markers using a vector geometry formulation of projection matrices”. *Physics in Medicine & Biology* 66.7 (2021). Publisher: IOP Publishing, p. 075013 (cit. on p. 69).
- [87] J. Gregor and T. Benson. “Computational analysis and improvement of SIRT”. *IEEE Transactions on Medical Imaging* 27.7 (2008), pp. 918–924 (cit. on pp. 9, 44, 46, 72, 73).
- [88] G. Van der Ham. “De boekenkist van Hugo de Groot (1621)”. In: *Verzameld verleden: veertig gedenkwaardige momenten en figuren uit de vaderlandse geschiedenis*. Verloren, Hilversum, 2004 (cit. on p. 52).
- [89] K. Haneca, R. d. Boodt, V. Herremanas, H. d. Pauw, J. V. Acker, C. v. d. Velde, and H. Beeckman. “Late Gothic Altarpieces As Sources of Information on”. *IAWA Journal* 26.3 (2005), pp. 273–298 (cit. on p. 51).
- [90] K. Haneca, K. Cufar, and H. Beeckman. “Oaks, tree-rings and wooden cultural heritage: a review of the main characteristics and applications of oak dendrochronology in Europe”. *Journal of Archaeological Science* 36.1 (2009), pp. 1–11 (cit. on p. 42).
- [91] L. Helfen, A. Myagotin, P. Mikulk, P. Pernot, A. Voropaev, M. Elyyan, M. D. Michiel, J. Baruchel, and T. Baumbach. “On the implementation of computed laminography using synchrotron radiation”. *Review of Scientific Instruments* 82 (2011), p. 063702 (cit. on p. 43).
- [92] L. Helfen, T. F. Morgeneyer, F. Xu, M. N. Mavrogordato, I. Sinclair, B. Schillinger, and T. Baumbach. “Synchrotron and neutron laminography for three-dimensional imaging of devices and flat material specimens”. 103 (2012), pp. 170–173 (cit. on p. 43).
- [93] K. Hiller. “Krummer Zink, gerade Stäbchen”. *Restauro* 8 (2018), pp. 34–38 (cit. on pp. 33, 36).
- [94] Y. Hou, M. Canul-Ku, X. Cui, and M. Zhu. “Super-resolution reconstruction of vertebrate microfossil computed tomography images based on deep learning”. *X-Ray Spectrometry* (2023), xrs.3389 (cit. on p. 59).
- [95] J. Hsieh. *Computed Tomography: Principles, Design, Artifacts, and Recent Advances*. SPIE PRESS, 2015 (cit. on pp. 5, 6, 24, 26).
- [96] J. Hwang, H. Kim, T. Lee, D.-i. Choi, T. Kwon, and S. Cho. “Geometry calibration for a dental cone-beam CT system with an offset detector”. *Precision Engineering* 79 (2023), pp. 264–276 (cit. on p. 69).
- [97] *Industrial 3D Scanner, Space Spider*. URL: <https://www.artec3d.com/portable-3d-scanners/artec-spider> (visited on Nov. 9, 2023) (cit. on p. 86).
- [98] P. P. Jaju, M. Jain, A. Singh, and A. Gupta. “Artefacts in cone beam CT”. *Open Journal of Stomatology* 03.05 (2013), pp. 292–297 (cit. on p. 26).

- [99] Y. S. N. Jayaratne, C. P. J. McGrath, and R. A. Zwahlen. “How Accurate Are the Fusion of Cone-Beam CT and 3-D Stereophotographic Images?” *PLOS ONE* 7.11 (2012). Publisher: Public Library of Science, e49585 (cit. on p. 79).
- [100] C. Johnson, E. Hendriks, I. Berezhnoy, E. Brevdo, S. Hughes, I. Daubechies, J. Li, E. Postma, and J. Wang. “Image processing for artist identification”. *IEEE Signal Processing Magazine* 25.4 (2008), pp. 37–48 (cit. on pp. 23, 41).
- [101] W. R. Johnston and S. Kelly. *Untamed. The Art of Antoine-Louis Barye*. Exhibition Catalogue. Baltimore: The Walters Art Museum, 2006 (cit. on p. 65).
- [102] G. van Kaick and S. Delorme. “Computed tomography in various fields outside medicine”. *European Radiology Supplements* 15.S4 (2005), pp. d74–d81 (cit. on pp. 5, 23, 59).
- [103] W. A. Kalender. “CT: the unexpected evolution of an imaging modality”. *European Radiology Supplements* 15.S4 (2005), pp. d21–d24 (cit. on pp. 24, 59).
- [104] F. Kharfi. “Mathematics and Physics of Computed Tomography (CT): Demonstrations and Practical Examples”. In: *Imaging and Radioanalytical Techniques in Interdisciplinary Research - Fundamentals and Cutting Edge Applications*. IntechOpen, 2013 (cit. on p. 126).
- [105] A. Kingston, A. Sakellariou, T. Varslot, G. Myers, and A. Sheppard. “Reliable automatic alignment of tomographic projection data by passive auto-focus”. *Medical Physics* 38.9 (2011), pp. 4934–4945 (cit. on p. 69).
- [106] M. Kiss, F. G. Bossema, P. J. Van Laar, S. Meijer, F. Lucka, T. Van Leeuwen, and K. J. Batenburg. “Beam filtration for object-tailored X-ray CT of multi-material cultural heritage objects”. *Heritage Science* 11, 130 (2023) (cit. on pp. 7, 8, 16, 60, 88, 100, 149).
- [107] N. Klop. *ICP (iterative closest point) registration / alignment - Blender Market*. URL: <https://blendermarket.com/products/icp-iterative-closest-point-registration-addon> (visited on Nov. 9, 2023) (cit. on p. 83).
- [108] A. Kostenko, W. Palenstijn, S. Coban, A. Hendriksen, R. van Liere, and K. Batenburg. “Prototyping X-ray tomographic reconstruction pipelines with FleXbox”. *SoftwareX* 11 (2020), p. 100364 (cit. on pp. 10, 28, 47, 65, 70, 128).
- [109] A. Kostenko, V. Andriiashen, and K. J. Batenburg. “Registration-based multi-orientation tomography”. *Optics Express* 26.22 (2018), p. 28982 (cit. on p. 28).
- [110] J. Lang and A. Middleton. *Radiography of Cultural Material*. Publication Title: Radiography of Cultural Material. Elsevier Butterworth-Heinemann, 2005 (cit. on pp. 23, 41).
- [111] A. Larsson. *Cybis CooRecorder - Image Coordinate Recording program & CDendro - Cybis dendro dating program*. 2017. URL: www.cybis.se (visited on Nov. 9, 2023) (cit. on p. 47).

- [112] S. Legrand, F. Vanmeert, G. Van der Snickt, M. Alfeld, W. De Nolf, J. Dik, and K. Janssens. “Examination of historical paintings by state-of-the-art hyperspectral imaging methods: from scanning infra-red spectroscopy to computed X-ray laminography”. *Heritage Science* 2.1 (2014) (cit. on pp. 23, 41, 43).
- [113] S. Longo, E. Mormina, F. Granata, D. Mallamace, M. Longo, and S. Capuani. “Investigation of an Egyptian Mummy board by Using Clinical Multi-slice Computed Tomography”. *Studies in Conservation* 63.7 (2018), pp. 383–390 (cit. on pp. 23, 24, 59).
- [114] M. Lüthi, B. A. Bircher, F. Meli, A. Küng, and R. Thalmann. “X-ray flat-panel detector geometry correction to improve dimensional computed tomography measurements”. *Measurement Science and Technology* 31.3 (2019). Publisher: IOP Publishing, p. 035002 (cit. on p. 69).
- [115] B. Masschaele, M. Dierick, D. V. Loo, M. N. Boone, L. Brabant, E. Pauwels, V. Cnudde, and L. V. Hoorebeke. “HECTOR: A 240kV micro-CT setup optimized for research”. In: *Journal of Physics: Conference Series*. Vol. 463. ISSN: 17426596 Issue: 1. 2013 (cit. on p. 27).
- [116] A. Masson-Berghoff and D. O’Flynn. “Absent, invisible or revealed ‘relics’? X-radiography and CT scanning of Egyptian bronze votive boxes from Naukratis and elsewhere”. *British Museum Studies in Ancient Egypt and Sudan* 24 (2019), pp. 159–174 (cit. on p. 26).
- [117] Maxon. *ZBrush*. URL: <https://www.maxon.net/en/zbrush> (visited on Nov. 9, 2023) (cit. on p. 78).
- [118] *Metropolitan-museum-of-art 3D models*. URL: <https://sketchfab.com/tags/metropolitan-museum-of-art> (visited on Nov. 9, 2023) (cit. on p. 78).
- [119] S. Mizuno, R. Torizu, and J. Sugiyama. “Wood identification of a wooden mask using synchrotron X-ray microtomography”. *Journal of Archaeological Science* 37.11 (2010), pp. 2842–2845 (cit. on pp. 24, 60).
- [120] V. Mocella, E. Brun, C. Ferrero, and D. Delattre. “Revealing letters in rolled Herculaneum papyri by X-ray phase-contrast imaging”. *Nature Communications* 6.1 (2015), p. 5895 (cit. on p. 23).
- [121] L. Montaina, S. Longo, G. Galotta, G. Tranquilli, R. Saccuman, and S. Capuani. “Assessment of the Panel Support of a Seventeenth-Century Dutch Painting by Clinical Multislice Computed Tomography”. *Studies in Conservation* 66.3 (2021), pp. 174–181 (cit. on pp. 24, 42, 60).
- [122] M. Mori, S. Kuhara, K. Kobayashi, S. Suzuki, M. Yamada, and A. Senoo. “Non-destructive tree-ring measurements using a clinical 3T-MRI for archaeology”. *Dendrochronologia* (2019) (cit. on p. 42).
- [123] M. P. Morigi, F. Casali, M. Bettuzzi, R. Brancaccio, and V. D’Errico. “Application of X-ray Computed Tomography to Cultural Heritage diagnostics”. *Applied Physics A* 100.3 (2010), pp. 653–661 (cit. on pp. 23, 24, 41, 59).

- [124] M. P. Morigi, F. Casali, A. Berdondini, M. Bettuzzi, D. Bianconi, R. Brancaccio, A. Castellani, V. D'Errico, A. Pasini, A. Rossi, C. Labanti, and N. Scianna. "X-ray 3D computed tomography of large objects: investigation of an ancient globe created by Vincenzo Coronelli". In: *O3A: Optics for Arts, Architecture, and Archaeology*. ISSN: 0277786X. 2007 (cit. on p. 60).
- [125] M. Morigi, F. Casali, M. Bettuzzi, D. Bianconi, R. Brancaccio, S. Cornacchia, A. Pasini, A. Rossi, A. Aldrovandi, and D. Cauzzi. "CT investigation of two paintings on wood tables by Gentile da Fabriano". *Nuclear Instruments and Methods in Physics Research Section A: Accelerators, Spectrometers, Detectors and Associated Equipment* 580.1 (2007), pp. 735–738 (cit. on p. 23).
- [126] H. A. Museums. *Prince Shōtoku: The Secrets Within*. URL: <https://harvardartmuseums.org/tour/prince-shotoku-the-secrets-within/slides/10799> (visited on Nov. 9, 2023) (cit. on pp. 23, 78).
- [127] K. Müller, M. Berger, J.-H. Choi, S. Datta, S. Gehrisch, T. Moore, M. P. Marks, A. K. Maier, and R. F. Müller. "Fully Automatic Head Motion Correction for Interventional C-arm Systems using Fiducial Markers". *Proceedings of the 13th Fully Three-Dimensional Image Reconstruction in Radiology and Nuclear Medicine* (2015), pp. 1–4 (cit. on p. 69).
- [128] V. Nguyen, J. De Beenhouwer, J. G. Sanctorum, S. Van Wassenbergh, S. Bazrafkan, J. J. J. Dirckx, and J. Sijbers. "A low-cost geometry calibration procedure for a modular cone-beam X-ray CT system". *Nondestructive Testing and Evaluation* 35.3 (2020), pp. 252–265 (cit. on p. 69).
- [129] P. Niemz and D. Mannes. "Non-destructive testing of wood and wood-based materials". *Journal of Cultural Heritage* 13.3 (2012), S26–S34 (cit. on pp. 23, 24).
- [130] L. N.M. Tissen. "3D Printing and the Art World: Current Developments and Future Perspectives". In: *Advances in 3D Printing*. Ed. by A. Sharma. IntechOpen, 2023 (cit. on p. 101).
- [131] *Numpy*. URL: <https://numpy.org/> (visited on Nov. 9, 2023) (cit. on p. 127).
- [132] D. Nykonenko, O. Yatsuk, L. Guidorzi, A. Lo Giudice, F. Tansella, L. P. Cesareo, G. Sorrentino, P. Davit, M. Gulmini, and A. Re. "Glass beads from a Scythian grave on the island of Khortytsia (Zaporizhzhia, Ukraine): insights into bead making through 3D imaging". *Heritage Science* 11.1 (2023), p. 238 (cit. on p. 13).
- [133] N. S. O'Brien, R. P. Boardman, I. Sinclair, and T. Blumensath. "Recent advances in X-ray cone-beam computed laminography". *Journal of X-Ray Science and Technology* 24 (2016), pp. 691–707 (cit. on p. 43).
- [134] T. Okochi. "A nondestructive dendrochronological study on japanese wooden shinto art sculptures using micro-focus X-ray Computed Tomography (CT): Reviewing two methods for scanning objects of different sizes". *Dendrochronologia* 38 (2016), pp. 1–10 (cit. on pp. 13, 42).

- [135] T. Okochi, Y. Hoshino, H. Fujii, and T. Mitsutani. “Nondestructive tree-ring measurements for Japanese oak and Japanese beech using micro-focus X-ray computed tomography”. *Dendrochronologia* 24.2-3 (2007), pp. 155–164 (cit. on pp. 12, 42).
- [136] R. Oliveira, A. de Paula, F. Gonçalves, R. Bueno, T. Calgam, S. Azeredo, O. Araújo, A. Machado, M. Anjos, R. Lopes, and D. Oliveira. “Development and characterization of a portable CT system for wooden sculptures analysis”. *Radiation Physics and Chemistry* (2022), p. 110409 (cit. on p. 60).
- [137] J. Padfield, D. Saunders, J. Cupitt, and R. Atkinson. “Improvements in the Acquisition and Processing of X-Ray Images of Paintings”. *National Gallery Technical Bulletin* 23 (2002), pp. 62–75 (cit. on p. 23).
- [138] K. Pande, J. J. Donatelli, D. Y. Parkinson, H. Yan, and J. A. Sethian. “Joint iterative reconstruction and 3D rigid alignment for X-ray tomography”. *Optics Express* 30.6 (2022), p. 8898 (cit. on p. 69).
- [139] D. Panetta, N. Belcari, A. D. Guerra, and S. Moehrs. “An optimization-based method for geometrical calibration in cone-beam CT without dedicated phantoms”. *Physics in Medicine & Biology* 53.14 (2008), p. 3841 (cit. on p. 69).
- [140] C. Parisi, C. Pelosi, U. Santamaria, P. Pogliani, G. Agresti, and S. Longo. “The conservation project of a liturgical object: The case of infant Jesus of Prague in the church of Saint Mary of providence at Macchia Giarre (Italy)”. *European Journal of Science and Theology* (2016) (cit. on pp. 13, 24).
- [141] E. M. Payne. “Imaging Techniques in Conservation”. *Journal of Conservation and Museum Studies* 10.2 (2013), pp. 17–29 (cit. on p. 23).
- [142] E. Pekel, F. Schaff, M. Dierolf, F. Pfeiffer, and T. Lasser. “X-ray computed tomography with seven degree of freedom robotic sample holder”. *Engineering Research Express* 4.3 (2022), p. 035022 (cit. on p. 69).
- [143] E. Petrella, S. Piciucchi, F. Feletti, D. Barone, A. Piraccini, C. Minghetti, G. Gruppioni, V. Poletti, M. Bertocco, and M. Traversari. “CT Scan of Thirteen Natural Mummies Dating Back to the XVI-XVIII Centuries: An Emerging Tool to Investigate Living Conditions and Diseases in History”. *PLOS ONE* 11.6 (2016). Ed. by J. Tuukkanen, e0154349 (cit. on pp. 24, 60).
- [144] M. Pieraccini, G. Guidi, and C. Atzeni. “3D digitizing of cultural heritage”. *Journal of Cultural Heritage* 2 (2001), pp. 63–70 (cit. on p. 77).
- [145] J. R. Pilcher. “Sample preparation, cross-dating and measurement”. In: *Methods of Dendrochronology: Applications in the Environmental Sciences*. Springer Science & Business Media, 1990, pp. 40–51 (cit. on p. 42).
- [146] R. Pintus, K. Pal, Y. Yang, T. Weyrich, E. Gobbetti, and H. Rushmeier. “A Survey of Geometric Analysis in Cultural Heritage: Geometric Analysis in Cultural Heritage”. *Computer Graphics Forum* 35.1 (2016), pp. 4–31 (cit. on pp. 23, 41).

- [147] S. T. Porter, N. Huber, C. Hoyer, and H. Floss. "Portable and low-cost solutions to the imaging of Paleolithic art objects: A comparison of photogrammetry and reflectance transformation imaging". *Journal of Archaeological Science: Reports* 10 (2016), pp. 859–863 (cit. on p. 77).
- [148] B. Raj, S. Ranganathan, and B. Venkatraman. "Non-Destructive Testing of Art Objects". In: *Reference Module in Materials Science and Materials Engineering*. Elsevier, 2017, B9780128035818022347 (cit. on p. 41).
- [149] A. Re, F. Albertin, C. Avataneo, R. Brancaccio, J. Corsi, G. Cotto, S. De Blasi, G. Dughera, E. Durisi, W. Ferrarese, A. Giovagnoli, N. Grassi, A. Lo Giudice, P. Mereu, G. Mila, M. Nervo, N. Pastrone, F. Prino, L. Ramello, M. Ravera, C. Ricci, A. Romero, R. Sacchi, A. Staiano, L. Visca, and L. Zamprotta. "X-ray tomography of large wooden artworks: the case study of "Doppio corpo" by Pietro Piffetti". *Heritage Science* 2.1 (2014), p. 19 (cit. on pp. 13, 23, 42).
- [150] A. Re, A. L. Giudice, M. Nervo, P. Buscaglia, P. Luciani, M. Borla, and C. Greco. "The importance of tomography studying wooden artefacts: A comparison with radiography in the case of a coffin lid from ancient Egypt". *International Journal of Conservation Science* 7.SI2 (2016), pp. 935–944 (cit. on pp. 13, 23, 41, 42).
- [151] C. Richmond. "Sir Godfrey Hounsfield". *BMJ* 329.7467 (2004), p. 687.1 (cit. on pp. 5, 23, 24).
- [152] Rigsters. *Multispectral Photogrammetry*. URL: <https://rigsters.com/portfolio/multispectral-photogrammetry/> (visited on Nov. 9, 2023) (cit. on p. 95).
- [153] Rijksmuseum. *Beurs van groen fluweel met trekkoord en afgezet met gouddraad op een doosje in de vorm van een schaar (fallus?) van dito fluweel en passemant, voorzien van twee metalen ogen, anonymous, after 1580*. URL: <https://www.rijksmuseum.nl/en/collection/BK-KOG-29> (visited on Nov. 9, 2023) (cit. on p. 14).
- [154] Rijksmuseum. *Book chest of Hugo de Groot, anonymous, c. 1600 - c. 1615*. URL: <https://www.rijksmuseum.nl/nl/collectie/NG-KOG-1208> (visited on Nov. 9, 2023) (cit. on pp. 14, 19, 52).
- [155] Rijksmuseum. *Bottle in the form of a shoe*. URL: <https://www.rijksmuseum.nl/en/collection/BK-KOG-1382> (visited on Nov. 9, 2023) (cit. on pp. 14, 90).
- [156] Rijksmuseum. *Cadmus, Guided by Minerva, Observes the Spartoi Fighting, Peter Paul Rubens (after), before 1747*. URL: <https://www.rijksmuseum.nl/en/collection/SK-A-4051> (visited on Nov. 9, 2023) (cit. on p. 14).
- [157] Rijksmuseum. *Cornett, anonymous, c. 1600 - c. 1650 - Rijksmuseum*. URL: <https://www.rijksmuseum.nl/en/collection/BK-AM-62-B> (visited on Nov. 9, 2023) (cit. on pp. 13, 14, 33, 36).

- [158] Rijksmuseum. *Langwerpig, taps toeopend foedraal met dop*. URL: <https://www.rijksmuseum.nl/nl/collectie/BK-NM-3086> (visited on Nov. 9, 2023) (cit. on pp. 8, 14, 16, 88).
- [159] Rijksmuseum. *Woman with Lantern (Midwife or Persian Sibyl), from a Nativity or Adoration of the Sheperds, anonymous, c. 1500 - c. 1515 - Rijksmuseum*. URL: <https://www.rijksmuseum.nl/en/collection/BK-NM-9253> (visited on Nov. 9, 2023) (cit. on pp. 2, 5, 14, 30, 31).
- [160] C. T. Rueden, J. Schindelin, M. C. Hiner, B. E. DeZonia, A. E. Walter, E. T. Arena, and K. W. Eliceiri. “ImageJ2: ImageJ for the next generation of scientific image data”. *BMC Bioinformatics* 18.1 (2017), p. 529 (cit. on p. 28).
- [161] L. Sabbatini and I. D. v. d. Werf. *Chemical Analysis in Cultural Heritage*. De Gruyter, 2020 (cit. on p. 41).
- [162] Z. Sabetsarvestani, B. Sober, C. Higgitt, I. Daubechies, and M. R. D. Rodrigues. “Artificial intelligence for art investigation: Meeting the challenge of separating x-ray images of the *Ghent Altarpiece*”. *Science Advances* 5.8 (2019), eaaw7416 (cit. on p. 23).
- [163] A. Sallam, S. Hemed, M. S. Toprak, M. Muhammed, M. Hassan, and A. Uheida. “CT Scanning and MATLAB Calculations for Preservation of Coptic Mural Paintings in Historic Egyptian Monasteries”. *Scientific Reports* 9.1 (2019), p. 3903 (cit. on p. 23).
- [164] U. Sass and D. Eckstein. “Preparation of large thin sections and surfaces of wood for automatic image analysis”. *Holzforschung* 48 (1994), pp. 117–118 (cit. on p. 47).
- [165] J. Schat, F. Bossema, M. E. Numans, I. Smeets, and P. Burger. “Overdreven gezondheidsnieuws: Relatie tussen overdrijving in academische persberichten en in nieuwsmedia”. *Nederlands Tijdschrift voor Geneeskunde* (2018) (cit. on p. 150).
- [166] J. Schindelin, I. Arganda-Carreras, E. Frise, V. Kaynig, M. Longair, T. Pietzsch, S. Preibisch, C. Rueden, S. Saalfeld, B. Schmid, J.-Y. Tinevez, D. J. White, V. Hartenstein, K. Eliceiri, P. Tomancak, and A. Cardona. “Fiji: an open-source platform for biological-image analysis”. *Nature Methods* 9.7 (2012), pp. 676–682 (cit. on pp. 11, 79).
- [167] D. Schorsch, L. Becker, and F. Caro. “Enlightened technology: Casting divinity in the Gupta age”. *Arts of Asia* 49.2 (2019), pp. 131–143 (cit. on p. 24).
- [168] R Schulze, U Heil, D Groß, D. Bruellmann, E Dranischnikow, U Schwanecke, and E Schoemer. “Artefacts in CBCT: a review”. *Dentomaxillofacial Radiology* 40.5 (2011), pp. 265–273 (cit. on pp. 26, 128).
- [169] F. Schweingruber. *Anatomie Europäischer Hölzer. - Anatomy of European Woods*. Haupt, 1990 (cit. on p. 63).
- [170] SCiem. *PAST4 – Personal Analysis System for Treering research*. 2009. URL: www.sciem.com (visited on May 2, 2021) (cit. on p. 47).

- [171] *Scikit Image - Canny Edge detector*. URL: https://scikit-image.org/docs/stable/auto_examples/edges/plot_canny.html (visited on Nov. 9, 2023) (cit. on p. 126).
- [172] *Scikit Image - Hough_circle*. URL: https://scikit-image.org/docs/stable/api/skimage.transform.html#skimage.transform.hough_circle (visited on Nov. 9, 2023) (cit. on p. 126).
- [173] *Scikit Image - Inpainting*. URL: https://scikit-image.org/docs/stable/auto_examples/filters/plot_inpaint.html (visited on Nov. 9, 2023) (cit. on p. 128).
- [174] *Scipy Optimize - Least_squares*. URL: https://docs.scipy.org/doc/scipy/reference/generated/scipy.optimize.least_squares.html (visited on Nov. 9, 2023) (cit. on p. 127).
- [175] M. M. Seger and P. E. Danielsson. “Scanning of logs with linear cone-beam tomography”. *Computers and Electronics in Agriculture* 41 (2003), pp. 45–62 (cit. on p. 43).
- [176] E. Y. Sidky, Y. Zou, and X. Pan. “Volume image reconstruction from a straight-line source trajectory”. *IEEE Nuclear Science Symposium Conference Record* 5 (2005), pp. 2441–2444 (cit. on p. 43).
- [177] A. T. d. Silva, S. Legrand, G. v. d. Snickt, R. Featherstone, K. Janssens, and G. Bottinelli. “MA-XRF imaging on René Magritte’s La condition humaine: Insights into the artist’s palette and technique and the discovery of a third quarter of La pose enchantée”. *Heritage Science* 5.1 (2017) (cit. on p. 23).
- [178] S. A. Sirr and J. R. Waddle. “Use of CT in Detection of Internal Damage and Repair and Determination of Authenticity in High-Quality Bowed Stringed Instruments”. *RadioGraphics* 19.3 (1999), pp. 639–646 (cit. on pp. 13, 24, 42).
- [179] *Sketchfab - The best 3D viewer on the web*. URL: <https://sketchfab.com> (visited on Nov. 9, 2023) (cit. on p. 78).
- [180] N. Sodini, D. Dreossi, A. Giordano, J. Kaiser, F. Zanini, and T. Zikmund. “Comparison of different experimental approaches in the tomographic analysis of ancient violins”. *Journal of Cultural Heritage* 27 (2017), S88–S92 (cit. on pp. 24, 42, 59).
- [181] J. Stelzner, F. Gauß, and P. Schuetz. “X-ray computed tomography for non-destructive analysis of early Medieval swords”. *Studies in Conservation* 61.2 (2016), pp. 86–101 (cit. on pp. 24, 26).
- [182] J. Stelzner and S. Million. “X-ray Computed Tomography for the anatomical and dendrochronological analysis of archaeological wood”. *Journal of Archaeological Science* 55 (2015), pp. 188–196 (cit. on pp. 12, 24, 42).
- [183] J. H. Stoner and R. Rushfield. *The Conservation of Easel Paintings*. Routledge: London and New York, 2012 (cit. on p. 41).
- [184] H. Strudwick and J. Dawson, eds. *Ancient Egyptian Coffins*. Oxbow Books, 2019 (cit. on p. 41).

- [185] P. Targowski, B. Rouba, M. Wojtkowski, and A. Kowalczyk. “The application of optical coherence tomography to non-destructive examination of museum objects”. *Studies in Conservation* 49.2 (2004) (cit. on p. 23).
- [186] M. Tesaxrová, E. Heude, G. Comai, T. Zikmund, M. Kaucká, I. Adameyko, S. Tajbakhsh, and J. Kaiser. “An interactive and intuitive visualisation method for X-ray computed tomography data of biological samples in 3D Portable Document Format”. *Scientific Reports* 9.1 (2019), p. 14896 (cit. on p. 95).
- [187] The British Museum. *mosaic; figure; vessel*. URL: https://www.britishmuseum.org/collection/object/E_Am-165 (visited on Nov. 9, 2023) (cit. on pp. 14, 87).
- [188] The British Museum. *mummy-mask*. URL: https://www.britishmuseum.org/collection/object/Y_EA29472 (visited on Nov. 9, 2023) (cit. on pp. 14, 92).
- [189] The British Museum (@britishmuseum). URL: <https://sketchfab.com/britishmuseum> (visited on Nov. 9, 2023) (cit. on p. 78).
- [190] The J. Paul Getty Museum. *Python Killing a Gnu, Antoine-Louis Barye*. URL: <https://www.getty.edu/art/collection/object/103RQ1> (visited on Nov. 9, 2023) (cit. on pp. 14, 20).
- [191] The See-through Museum. URL: <https://www.nwo.nl/projecten/341-60-001-0> (visited on Nov. 9, 2023) (cit. on p. 25).
- [192] Thermo Fisher. *Avizo Software / Materials Characterization Software - NL*. URL: <https://www.thermofisher.com/uk/en/home/electron-microscopy/products/software-em-3d-vis/avizo-software.html> (visited on Nov. 9, 2023) (cit. on pp. 11, 79).
- [193] J. Thornton, N. Umney, G. Landrey, M. Baumester, and S. May. “Other materials and structures”. In: *Conserv. Furnit.* 2007, pp. 194–237 (cit. on p. 26).
- [194] *Trackpy*. URL: <http://soft-matter.github.io/trackpy/v0.3.0/index.html> (visited on Nov. 9, 2023) (cit. on p. 126).
- [195] C. Tuniz, F. Bernardini, I. Turk, L. Dimkaroski, L. Mancini, and D. Dreossi. “Did neanderthals play music? X-ray computed micro-tomography of the divje babe ‘flute’”. *Archaeometry* 54.3 (2012), pp. 581–590 (cit. on p. 24).
- [196] M. Vandenbeusch, D. O’Flynn, and B. Moreno. “Layer by Layer: The Manufacture of Graeco-Roman Funerary Masks”. *The Journal of Egyptian Archaeology* 107.1-2 (2021), pp. 281–298 (cit. on pp. 59, 60, 78, 79).
- [197] A. Vandivere, A. van Loon, K. A. Dooley, R. Haswell, R. G. Erdmann, E. Leonhardt, and J. K. Delaney. “Revealing the painterly technique beneath the surface of Vermeer’s Girl with a Pearl Earring using macro- and microscale imaging”. *Heritage Science* 7.1 (2019), p. 64 (cit. on pp. 23, 41).

- [198] A. Vannoppen, S. Maes, V. Kint, T. De Mil, Q. Ponette, J. Van Acker, J. Van den Bulcke, K. Verheyen, and B. Muys. "Using X-ray CT based tree-ring width data for tree growth trend analysis". *Dendrochronologia* 44 (2017), pp. 66–75 (cit. on p. 24).
- [199] D. Vavrik, V. Antuskova, S. Chlumska, I. Kumpova, R. Sefcu, and M. Vopalsky. "Non-destructive exploration of late Gothic panel painting using X-ray tomography and flattening of the reconstructed data". *The European Physical Journal Plus* 138.7 (2023), p. 618 (cit. on p. 60).
- [200] C. Villa, M. J. Flies, and C. Jacobsen. "Forensic 3D documentation of bodies: Simple and fast procedure for combining CT scanning with external photogrammetry data". *Journal of Forensic Radiology and Imaging* 12 (2018), e2–e7 (cit. on p. 79).
- [201] Volume Graphics. *VGSTUDIO*. URL: <https://www.volumegraphics.com/en/products/vgstudio.html> (visited on Nov. 9, 2023) (cit. on pp. 11, 79).
- [202] R. Wagner, T. Fuchs, G. Scholz, C. Kretzer, R. Schielein, M. Firsching, S. Kirsch, M. Wolters, M. Raquet, and F. P. Bär. "Dual-energy computed tomography of historical musical instruments made of multiple materials." In: *8th Conference on Industrial Computed Tomography*. 2018 (cit. on p. 42).
- [203] P. Xin, H. Yu, H. Cheng, S. Shen, and S. G. F. Shen. "Image Fusion in Craniofacial Virtual Reality Modeling Based on CT and 3dMD Photogrammetry". *Journal of Craniofacial Surgery* 24.5 (2013), p. 1573 (cit. on p. 79).
- [204] K. Yang, A. L. C. Kwan, D. F. Miller, and J. M. Boone. "A geometric calibration method for cone beam CT systems: A geometric calibration method for cone beam CT". *Medical Physics* 33.6Part1 (2006), pp. 1695–1706 (cit. on p. 69).
- [205] Y. Yang, L. Li, and Z.-Q. Chen. "A review of geometric calibration for different 3-D X-ray imaging systems". *Nuclear Science and Techniques* 27.3 (2016), p. 76 (cit. on p. 69).
- [206] R. Yin, B. Cornelis, G. Fodor, N. Ocon, D. Dunson, and I. Daubechies. "Removing Cradle Artifacts in X-Ray Images of Paintings". *SIAM Journal on Imaging Sciences* 9.3 (2016), pp. 1247–1272 (cit. on p. 23).
- [207] F. Zhang, J. Du, H. Jiang, L. Li, M. Guan, and B. Yan. "Iterative geometric calibration in circular cone-beam computed tomography". *Optik* 125.11 (2014), pp. 2509–2514 (cit. on pp. 69, 83).
- [208] T. Zhang, Y. Xing, L. Zhang, X. Jin, H. Gao, and Z. Chen. "Stationary computed tomography with source and detector in linear symmetric geometry: Direct filtered backprojection reconstruction". *Medical Physics* 47.5 (2020), pp. 2222–2236 (cit. on p. 43).
- [209] X. Zhang, J. Blaas, C. Botha, P. Reischig, A. Bravin, and J. Dik. "Process for the 3D virtual reconstruction of a microcultural heritage artifact obtained by synchrotron radiation CT technology using open source and free software". *Journal of Cultural Heritage* 13.2 (2012), pp. 221–225 (cit. on p. 23).

-
- [210] J. Zhou, M. Maisl, H. Reiter, and W. Arnold. “Computed laminography for materials testing”. *Applied Physics Letters* 68.24 (1996), pp. 3500–3502 (cit. on p. 43).

A

Appendix A:

Supplementary information

This appendix contains the supplementary information to chapter 4. In this appendix we extend upon the methods and implementation.

A.1 Supplementary methods

A.1.1 Model and optimisation

In this section we discuss the theory and model that underlies the implementation of our marker-based system parameter derivation. In less sophisticated X-ray imaging equipment, these parameters are often not available. By including small metal balls in the acquisition, we retrieve these parameters based on the radiographs. Each marker is visible as a circle on all (or most) projections, and we call its location the projected marker location (PML). For each marker we measure the PML on the X-ray images. Given a set of system parameters and marker positions, and for each marker at each rotation angle, we can draw a line from the source through the marker. The intersection of this line with the detector plane gives a predicted PML. The goal is to minimise the distance between the predicted PMLs and the measured PMLs. This will provide an estimated value for the system parameters, which we need for 3D reconstruction as described in section 4.3.

We aim to find parameters that can be used to produce a 3D reconstruction of the object. Our method does not aim to find the absolute physical distances. The only impact of this on the 3D reconstruction is the scale, which can if needed be obtained by including an object of known size in the scan or by measuring one distance on the object afterwards and scaling the reconstruction accordingly. In the next sections, we will first discuss the model used for the forward projection of marker positions and then the optimisation that is used for estimating the system parameters.

This is the appendix to chapter 4 and is published as Supplementary Information to F. G. Bossema, W. J. Palenstijn, A. Heginbotham, M. Corona, T. Van Leeuwen, R. Van Liere, J. Dorscheid, D. O'Flynn, J. Dyer, E. Hermens, and K. J. Batenburg. "Enabling 3D CT-scanning of cultural heritage objects using only in-house 2D X-ray equipment in museums". *Nature Communications* (accepted, in press).

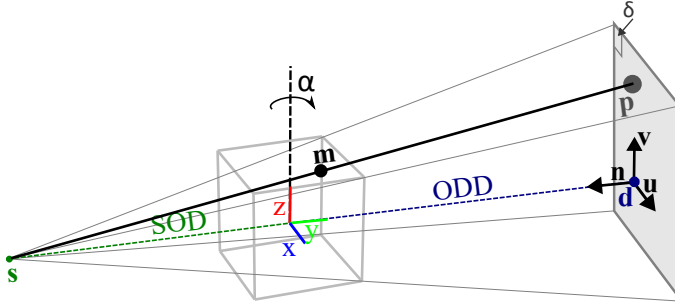


Figure A.1: Schematic indicating the variables and notation used in the forward model.

The forward model

We assume that the setup consists of a cone-beam X-ray source, flat-panel detector and a rotation stage. A block of foam containing markers is mounted on the rotation stage next to the object. We assume that the components are stably mounted and do not drift during acquisition. For our calculations, we model the system as the source and detector rotating around the object, which is mathematically equivalent to a rotating object between a static source and detector.

We define a left handed coordinate system with the rotation axis being the z -axis. The y -axis is defined such that the source lies on it for the first projection. The first projection is defined as rotation angle 0° . The coordinate system and variables used to describe all the system components are shown in figure A.1.

A boldface small letter represents a vector with an x , y and z component, e.g. $\mathbf{s} = (s_x, s_y, s_z)$, which represents the location of the source. The detector plane is defined by a point \mathbf{d} , which is the center of the detector plane, the detector pixel size and the unit vectors \mathbf{u} and \mathbf{v} that span the detector plane. The normal vector to the detector plane is $\mathbf{n} = \mathbf{v} \times \mathbf{u}$. The out-of-plane rotations of the detector are given by angles θ (around axis \mathbf{u}) and ϕ (around axis \mathbf{v}). The parameter η defines the in-plane detector rotation (rotation around \mathbf{n}). With a subscript i , e.g. \mathbf{s}_i , we denote the vector that is obtained when rotating the original vector around the z -axis by angle $-\alpha_i$. The marker position of marker j is denoted by $\mathbf{m}_j = (m_{jx}, m_{jy}, m_{jz})$ for $j \in \{1, \dots, N\}$.

A line from the source through marker j for projection i is given as $\mathbf{f}(t) = \mathbf{s}_i + t(\mathbf{m}_j - \mathbf{s}_i)$. The vector defining the projected 3D location in space of the PML corresponding to marker j on projection i , is given by the intersection of this line with the detector plane defined by \mathbf{d}_i and \mathbf{n}_i : $\mathbf{g} = \mathbf{s}_i + \frac{\mathbf{n}_i \cdot (\mathbf{d}_i - \mathbf{s}_i)}{\mathbf{n}_i \cdot (\mathbf{m}_j - \mathbf{s}_i)}(\mathbf{m}_j - \mathbf{s}_i)$. This 3D location can be rewritten to the detector pixel on which the marker would fall. In other words, we obtain the PML $\mathbf{p}_{i,j}^{pred}(\Theta, \mathbf{m}_j) = (a, b)$ (row, column) such that $\mathbf{d}_i + a\mathbf{u}_i + b\mathbf{v}_i = \mathbf{g}$.

Parameter	Notation
detector position	\mathbf{d}
detector tilt	θ, ϕ
detector in-plane rotation	η
projection angles	$\alpha_1, \dots, \alpha_{n-1}$
marker positions	$\mathbf{m}_1, \dots, \mathbf{m}_N$

Table A.1: Notation of the free system parameters and marker positions \mathbf{m} that are estimated in the optimisation scheme.

Parameter	Notation and fixed value
source position	$\mathbf{s}_0 = (0, SOD, 0)$
first projection angle	$\alpha_0 = 0$
detector pixel size	$\delta = \text{detector pixel size}$

Table A.2: Fixed system parameters. The source to object distance (SOD) and detector pixel size are user input.

The cost function

The measured PML \mathbf{p}_{ij}^{meas} of marker j on projection image i , is defined relative to \mathbf{d}_i and is given by (c, d) (row, column).

The set of free parameters, which we for convenience denote by Θ , define the forward projections. The free parameters are given in Supplementary table A.1 and the fixed parameters in Supplementary table A.2. The source is fixed to the negative y -axis. We fix the detector pixel size, since this is often specified in the documentation of the manufacturer. We want to minimise the distance between the predicted PML $\mathbf{p}_{ij}^{pred}(\Theta, \mathbf{m}_j)$ and the measured PML \mathbf{p}_{ij}^{meas} of marker j on projection image i . We therefore want to find the parameters Θ and \mathbf{m}_j , $j \in \{1, \dots, N\}$ that minimise the following:

$$\sum_i \sum_j |\mathbf{p}_{ij}^{meas} - \mathbf{p}_{ij}^{pred}(\Theta, \mathbf{m}_j)|^2. \quad (\text{A.1})$$

A.1.2 Implementation

The proposed workflow consists of six steps (figure A.2), the first two are the practical data acquisition phase which takes place in the X-ray suite:

1. Object and marker holder preparation;
2. Data acquisition;

After data acquisition the computational workflow consist of the following steps:

1. Marker detection and labelling;
2. System parameter derivation;
3. Pre-processing and Inpainting;
4. 3D reconstruction.

In the following sections we expand on each of these steps.

Data acquisition in the X-ray suite

Object and marker holder preparation

First, a marker holder is made by inserting a number of markers into two or more pieces of foam. The size and shape can be arbitrary, the holder can be adjusted to the size and shape of the object. They should be distributed vertically to limit the overlap of the projected markers on the radiographs. The object is mounted on the rotation stage, the marker holder is placed next to it. Using the live radiographic inspection, the positions of the markers are checked and adjusted if needed.

Although a full discussion of the requirements of the positions of the markers within the foam is beyond the scope of this article, here we give some general guidelines. For an accurate parameter estimation, the markers should be distributed within the foam in three dimensions so that they span the detector field of view where the object is located. If the markers are on one vertical line for example, the depth information is not captured in their positions as well as when they are distributed. This is due to the fact that the trajectory of the markers on the detector forms an ellipse and therefore movement of the PML (and the corresponding geometric information gain) is less on the sides of the ellipse than in the center. The number of markers needs to be sufficient for the system of equations to be resolved. In practice, it is advisable to take more markers where possible, since the contrast with the object may not always be sufficient to find all markers in each radiograph or they rotate out of the field of view for a few radiographs. The overlap of markers on the radiographs should be avoided, because this hampers the correct labelling of the markers. Therefore, we distribute the markers vertically to limit overlap on radiographs. Since the rotation angles are part of the parameter set, in each radiograph markers should be present. For the scans in chapter 4, we have used a minimum distance between markers of 1cm. We have moreover used the live radiographic inspection to ensure as few projections as possible had overlapping markers. This facilitates the labelling and tracking of the markers. We used 10 markers for the wooden block and 17 markers for the case study.

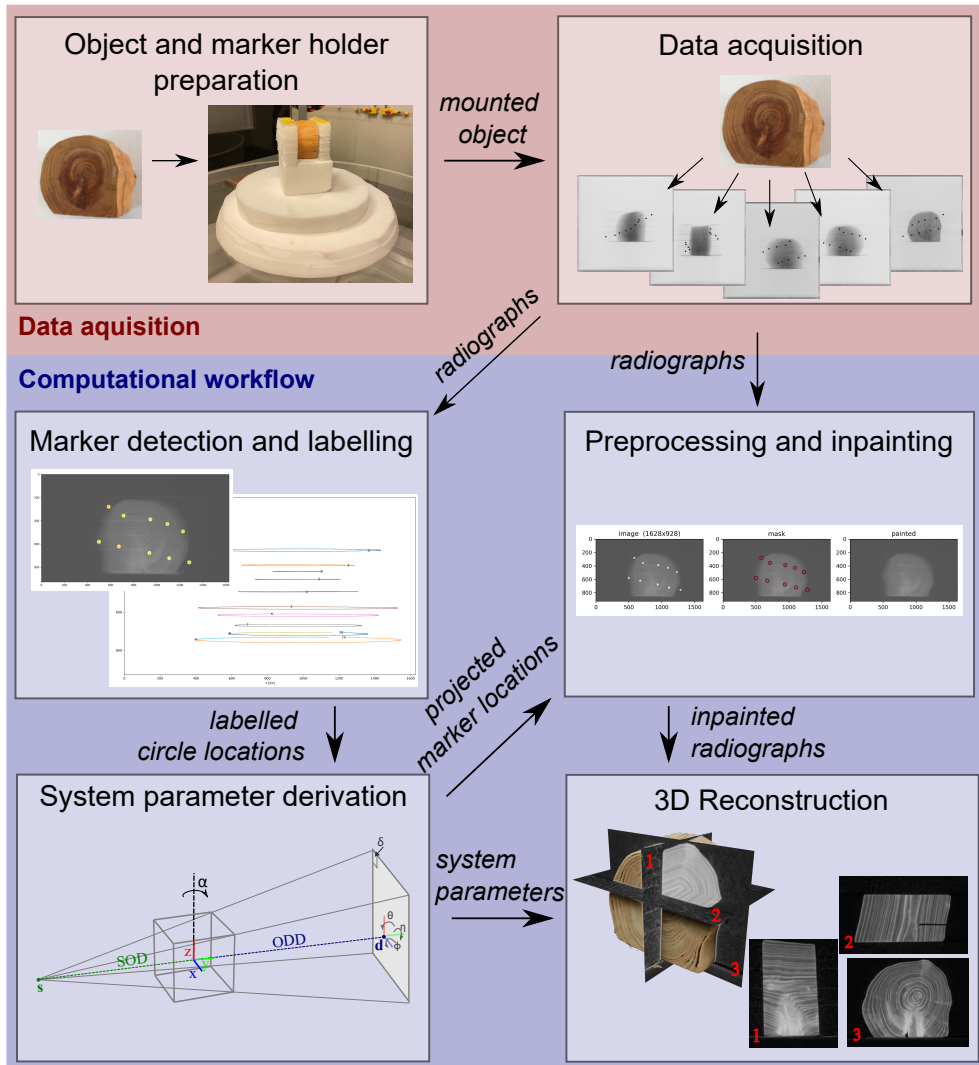


Figure A.2: Steps in the post-scan marker-based parameter derivation method for 3D reconstruction.

The following steps can be used to setup the markerholder:

1. Place the markers in two or more pieces of foam, keeping them at least 1cm apart and avoiding placing them on a straight line. The number of markers will depend on the size of the object and the magnification, since the main goal is to have no overlapping markers on the radiographs. See figure A.3a.
2. Place the pieces of foam on the rotation stage, next to the mounted object. If convenient, placing two at 90° gives a good spread of the markers on the detector view. See figure A.3b,c.
3. Turn on live radiographic inspection of the object and markers and determine the maximum magnification that ensures the object stays in the field of view during rotation. See figure A.3d.
4. Make sure that during rotation there is no radiograph on which no markers are visible. Markers can rotate out of the field of view, but in every radiograph markers need to be present.
5. If there are radiographs in which the markers overlap, try to increase the vertical space between markers until they do not overlap.



Figure A.3: Preparing the markerholder. a) Including markers in foam. b) Placing foam next to the wooden block. c) Placing the wooden block and markerholder on the rotation stage at the Rijksmuseum. d) Resulting radiograph in the Rijksmuseum facility.

Data acquisition

Radiographs are collected over one or more revolutions of the rotation stage. A flatfield, an image with the source turned on without an object in view, and darkfield, an image with the source off, are collected for the pre-processing step [104].

Computational workflow

Marker detection and labelling

The computational workflow starts with measuring the PML on the projections, by first using the Canny Edge detector [171] and consequently an implementation of the Hough Transform to identify circles from the Scikit toolbox [172]. Making use of the Trackpy toolbox [194], we identify the same projected marker from projection to projection, forming the ellipse shaped trajectory followed by the projected marker (step 2 in figure A.2). Both locating and labelling may require user input, as the locating of projected marker on the image depends on the total brightness and contrast and wrongly labelled projected markers can make parameter estimation less reliable. During the locating step some dense features in the object may be identified as projected markers that do not correspond to markers. When the markers overlap with the

object or rotate out of the field of view, the corresponding projected markers may not be found in a number of projections. This causes errors in the labelling step. These errors are reduced by filtering out short trajectories, determining a maximum step size for the projected marker from projection to projection and a memory parameter that determines for how many projections a marker can be missing to still belong to the same label. These parameters can be influenced by the user based on visual inspection of the resulting trajectories. It is preferable to have a trajectory cut into multiple labels over mislabelling (e.g. crossover of labels between two markers). The number of found labels is N^* . Note that this can be a higher number than the actual number of markers N , due to features in the object being identified as projected markers or partially labelled trajectories, or a lower number due to non-identified projected markers in the locating step. During the optimisation in the next step this is taken into account.

System parameter estimation

The System parameter estimation algorithm is given in Algorithm 1. It consists of two optimisation steps with a marker merging step in between. The required user input is the detector pixel size (δ) and an estimation of the source to object distance (SOD). This source position is used to fix the location of the source at distance SOD from the rotation axis on the negative y -axis (see section A.1.1). The resulting reconstruction will therefore be scaled relative to this given SOD.

To provide an educated initial guess on the system parameters, further input is requested from the user: estimated values for the ODD, the number of revolutions (n_{rounds}) of the rotation stage and the approximate average distance r of the markers to the rotation center. These inputs are used to create the following initialisation: i) The detector is placed on the positive y -axis at distance ODD from the origin, ii) the detector tilts and skew are 0, iii) projection angles are equidistant over $2\pi n_{rounds}$ (radians) and iv) the initial marker locations are placed randomly within a ball with radius r , their labels based on their vertical location. This initial guess and the residual function described by equation A.1 are input for the `scipy.optimize` package's `least_squares` function [174]. Derivatives are calculated using an automated derivative package `autograd` [10], that is a wrapper for `numpy` [131].

For each iteration a reduced number of projected markers per projection image are used, to make the method robust against mislabelled markers. Projected markers are selected that have the lowest distance of the predicted PML to the measured PML. In other words, we use labels $h_i(\Theta, N_k)$, which are the N_k labels j with smallest $|\mathbf{p}_{ij}^{meas} - \mathbf{p}_{ij}^{pred}(\Theta, \mathbf{m}_j)|$. The number of projected markers that are used in the first and second optimisation step are given by N_1 and N_2 and are input by the user. The least squares optimisation terminates when the step size or cost function improvement are below a given threshold of 10^{-6} . The user can give an upper limit n_{iter1} and n_{iter2} for the number of iterations of the least squares solver in the first and second optimisation step respectively. In the marker merging step a minimum distance between marker positions is used to decide whether or not to merge two labels. This distance can be chosen by the user.

Algorithm 1 System parameter estimation.

- 1: **Initial Guess.** The initial guess is defined by a standard circular scan with equidistant angles and the user input values ODD, n_{rounds} and r .
- 2: **First optimisation.** Run least squares optimisation starting from the initial guess until thresholds are reached or until the number of iterations exceeds n_{iter1} , to find the parameters (Θ^* and $\mathbf{m}_1^*, \dots, \mathbf{m}_N^*$) that minimise the following value

$$\sum_i \sum_{j \in h_i(\Theta^*, N_1)} |\mathbf{p}_{ij}^{meas} - \mathbf{p}_{ij}^{pred}(\Theta^*, \mathbf{m}_j^*)|^2.$$

- 3: **Merge markers.** If the distance between the positions of two markers $|\mathbf{m}_j - \mathbf{m}_k|$ is smaller than a given threshold and do not overlap for more than a given number of frames, the labels j, k refer to the same projected marker and their trajectories are merged, or in other words k is relabelled j and removed. N^{**} denotes the number of labels after this merging step.
- 4: **Updated initial guess** Use Θ^* and $\mathbf{m}_j^*, j \in \{1, \dots, N^{**}\}$ as updated initial guess for the second optimisation step.
- 5: **Second optimisation.** Run least squares optimisation starting from the initial guess until thresholds are reached or until the number of iterations exceeds n_{iter2} , to find the parameters (Θ^{**} and $\mathbf{m}_1^{**}, \dots, \mathbf{m}_N^{**}$) that minimise the following value

$$\sum_i \sum_{j \in h_i(\Theta^{**}, N_2)} |\mathbf{p}_{ij}^{meas} - \mathbf{p}_{ij}^{pred}(\Theta^{**}, \mathbf{m}_j^{**})|^2.$$

- 6: **Calibrated parameters.** Return Θ^{**} .

Pre-processing and inpainting

The recorded data is first flat- and darkfield corrected. Using the system parameters and marker positions found in the previous step, a forward projection is performed to obtain the predicted PML locations on all the projections. These are used to algorithmically remove the projections of the markers on the radiographs by the inpainting function of the scikit-image package [173], because high density material in a CT acquisition can cause image artefacts in the reconstruction [168]. It is possible to perform both a reconstruction with the original radiographs and the inpainted radiographs. Therefore the user can choose which reconstruction serves them best, since the effect of inpainting can differ per object and placement of the markers.

3D reconstruction

The inpainted projections, together with the system parameters resulting from the optimisation step are used to obtaining a 3D reconstruction. Because of the fixed source position, the solution that is obtained, is a scaled reconstruction. The estimated system parameters are transformed into a geometry description that is then used within the SIRT algorithm provided by the FleX-box toolbox [108] to make a 3D reconstruction of the object.

A.2 Supplementary figures and tables

A.2.1 Parameters

In Supplementary table A.3 the computed system parameters of the scans of the wooden block are given. In figure A.4 the found angles for each system are given. We see that the British Museum setup provides equidistant angles and the other two systems have less regular angular intervals.

System parameters	BM system	BM markers	GM markers	RM markers	FlEx-ray
source location (mm)	(0.881,0)	(0.881,0)	(0, 881, 0)	(0.500,0)	(0.658,02,0)
detector location (mm)	(-31.46, 1362.0, 0)	(-31.32, 1471.44, -3.84)	(-32.97, 1351.04, -6.71)	(-2.63, 583.97, 2.78)	(0.430,98,0)
detector tilts (radians)	0, 0	0.027, 0.019	-0.004, 0.015	0.021, 0.001	0.0, 0.0
detector in-plane rotation	0.0	0.0	0.0	-0.002	-0.004

Table A.3: System parameters as reported by the system feedback (BM system) or the marker-based parameter retrieval (BM markers, GM markers, RM markers) for the scans of the wooden block (section 4.1.2). The source location is an estimate given by the user.

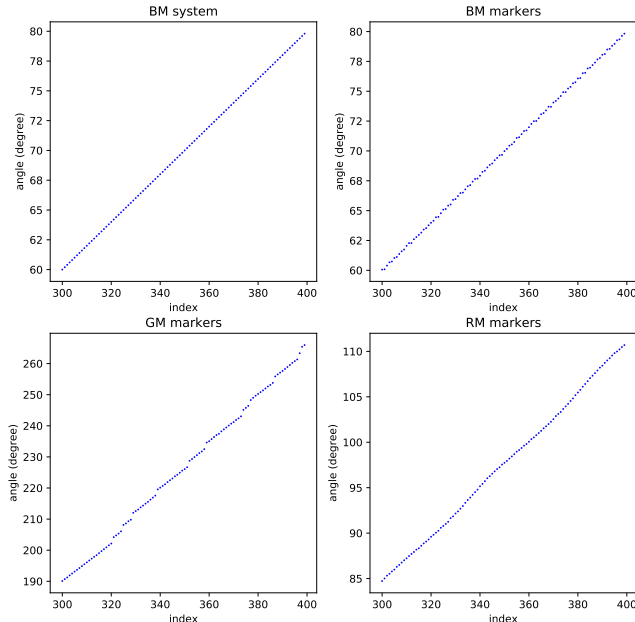


Figure A.4: Subset of the acquisition angles (index vs. angle (degrees)) of the test scans of the wooden block (main article section (section 4.1.2)), given by the British Museum system (BM system) and calculated by the marker-based parameter derivation at the British Museum (BM markers), The J. Paul Getty Museum (GM markers) and the Rijksmuseum (RM markers).

To investigate the accuracy and precision of the found marker positions, we performed simulation experiments. We simulated projected marker locations (PMLs) by forward projecting 3D marker locations. To simulate an incorrectly found center of the PML, we added gaussian noise with mean 0 and standard deviation from 0 up to 5 pixels to the PML. Next, we ran our parameter retrieval optimisation to obtain estimated 3D marker locations. Since our method does not assume the projection angles and other system parameters are known, the found 3D marker locations may have a slightly different orientation, vertical position, and scaling compared to the original marker positions. These variations do not affect the reconstruction quality, so to be able to measure the quality of the found marker locations, we compensate for them before comparing the found marker locations with the original marker locations used for the forward projection. For each choice of standard deviation, we ran this simulation with ten different random seeds, which influences the noise added to the PMLs, to obtain figure A.5 showing standard deviation (in pixels) versus the average error in the calculated marker positions (in mm). The average error is lower than the voxel size (0.13mm) except for a few outliers. In the practical datasets included in the manuscript, we found that the PML identification can be trusted to locate the centers within this error range.

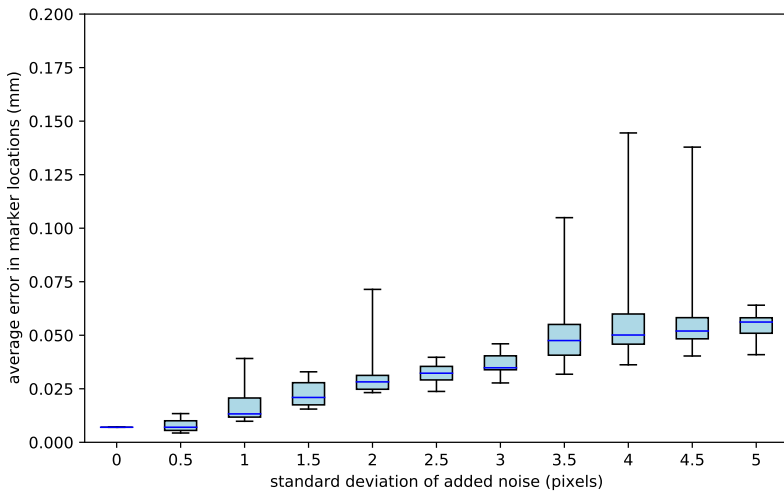


Figure A.5: Results of the simulation experiment. Boxplot showing average errors in the calculated marker positions (y-axis) when adding gaussian noise to the PML (standard deviation of noise on the x-axis). The boxplot shows the median (blue line), interquartile range (lightblue box), which shows where 50% of the data points around the median fall, and minima and maxima of the data (black horizontal bars).

A.2.2 Comparison of the marker based approach and FDK

Here we show the type of image artefacts that can be encountered when an imperfect calibration is used for a CT reconstruction. In figure A.6 a slice from a reconstruction of the wooden block dataset recorded at the J. Paul Getty museum is shown using the approach outlined in the main text and using a straightforward FDK approach with the angles estimated to be equidistant. The irregularity of the angular interval produces wrongly back-projected radiographs in the second reconstruction, showing the need for estimating the individual angular intervals. In figure A.7 we show the effect of errors in the rotation speed. Here, these effects are shown on a dataset of the wooden block recorded at a micro-CT facility, the FleX-ray laboratory, located at the Center for Mathematics and Computer Science in Amsterdam. For figure A.7 we removed angles at the end of the full rotation to simulate a slower rotation speed.

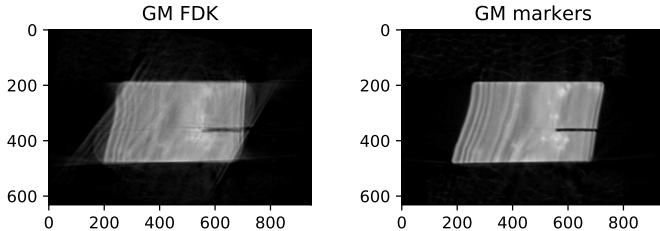


Figure A.6: Comparing the marker-based parameter retrieval method with a straightforward FDK reconstruction. A slice from the reconstruction of the dataset of the wooden block at the J. Paul Getty Museum with a) marker-based parameter retrieval and b) FDK with the angles estimated to be equidistant.

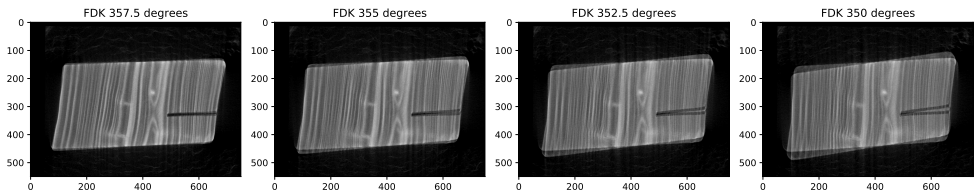


Figure A.7: Effect of lower rotation speed on FDK reconstruction. Here we show an FDK reconstruction where the rotation stage does not fully rotate to 360 degrees during one acquisition, reaching from left to right only 357.5, 355, 352.5 and 350 degrees, respectively, while the reconstruction incorrectly assumes that the rotation was over the full 360 degrees. The slower the rotation stage the larger the effect on the FDK reconstruction.

A.2.3 Inpainting

In figure A.8 we show a radiograph from the dataset of the wooden block, recorded at the FleX-ray laboratory, the mask used for inpainting and the inpainted radiograph. In figure A.9 a slice from a reconstruction of the wooden block dataset recorded at the FleX-ray laboratory is shown using the original radiographs and the inpainted radiographs. The effect of the inpainting on the reconstruction of the wooden block is visible in a blurring on the left side of the wooden block. The effect of the inpainting is dependent on the magnification. Since this is a high resolution scan, the magnification is large and therefore the marker shades a larger portion of the object than when the magnification is smaller. In figure A.10 we show the effect of the inpainting on the dataset recorded at the J. Paul Getty museum. Here the effect is small. Thus, the effect of inpainting depends on the settings. Whether to use the original or inpainted radiographs can be decided by the user upon inspection of the reconstructions.

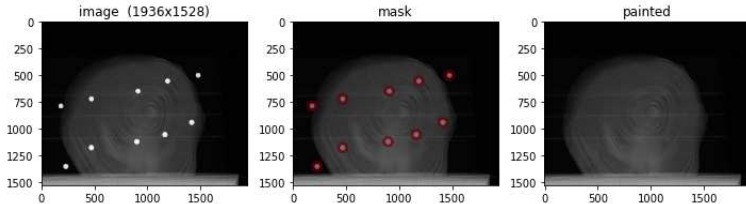


Figure A.8: Inpainting of the radiographs. A radiograph of the wooden block at the FleX-ray laboratory: original radiograph (left) and an overlay of the mask used for inpainting (in red) on the radiograph (middle) and resulting inpainted radiograph (right).

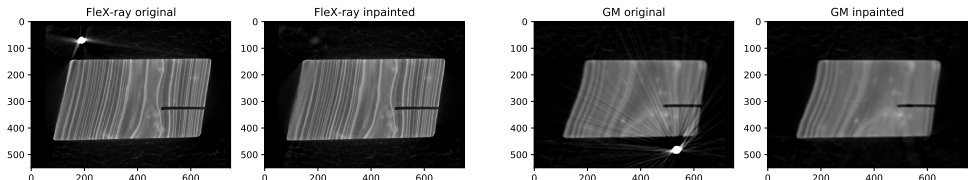


Figure A.9: Comparing reconstructions with and without inpainting. A slice from the reconstruction of the dataset of the wooden block at the FleX-ray laboratory with original radiographs (left) and inpainted radiographs (right).

Figure A.10: Comparing reconstructions with and without inpainting. A slice from the reconstruction of the dataset of the wooden block at the J. Paul Getty museum, using the marker based approach with a) original radiographs and b) inpainted radiographs.

B

Appendix B:

Intact user guidelines

This appendix to chapter 5 gives the user guidelines for the Intact plugin presented in that chapter.

B.1 Installation

B.1.1 Blender

Installation:

1. Go to <https://www.blender.org/download/> and pick the relevant version for your operating system and install.

Why Blender?

- Open source: Blender has a large community with plugins that could perhaps sustain future questions/demands of the INTACT tool.
- Old versions will stay available, so the plugin doesn't have to be updated for compatibility with future updates of Blender.
- Blender is based on Python. It is therefore easy to write and incorporate your own demands, and possible for any user to edit those based on their own needs.

This is the appendix to chapter 5 and has been published as Supplementary Material to F. G. Bossema, P. J. Van Laar, K. Meechan, D. O'Flynn, J. Dyer, T. Van Leeuwen, S. Meijer, E. Hermens, and K. J. Batenburg. "Inside out: Fusing 3D imaging modalities for the internal and external investigation of multi-material museum objects". *Digital Applications in Archaeology and Cultural Heritage* 31 (2023), e00296.

B.1.2 Blender plugin – INTACT

Installation:

1. Download the plugin here: 10.5281/zenodo.8041844 or clone the github repository.
2. Open Blender
3. Go to “edit -> preferences” (figure B.1)
4. Go to “add-ons” and click "install" (figure B.2)
5. Navigate to the INTACT_Windows_main.zip file and select it. Blender will now automatically install the plugin. Make sure to activate it by checking the box next to the plugin name. (figure B.3)
6. The INTACT plugin is now installed within your Blender software. You can find it in the UI Side Panel. Open this panel by clicking the little arrow next to the orientation gimbal. (figure B.4) and then choose the INTACT panel (figure B.5).
7. When opening the INTACT panel, you'll be prompted to click a button ‘Install Modules’. Do this. When it's done close blender and restart.

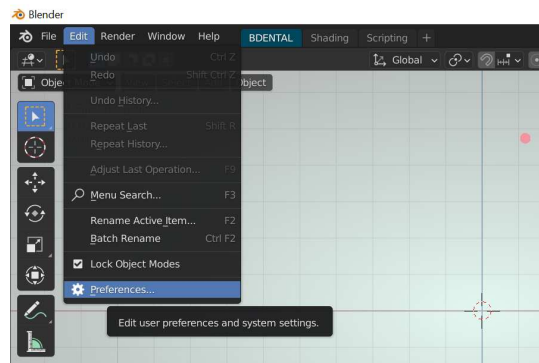


Figure B.1

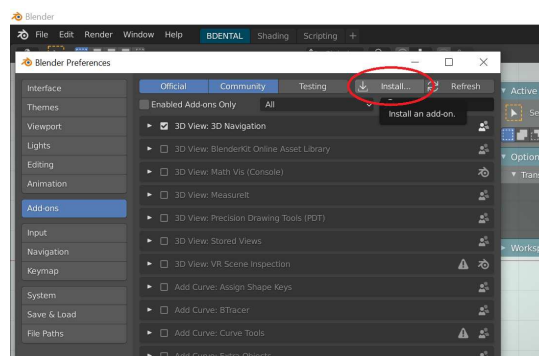


Figure B.2

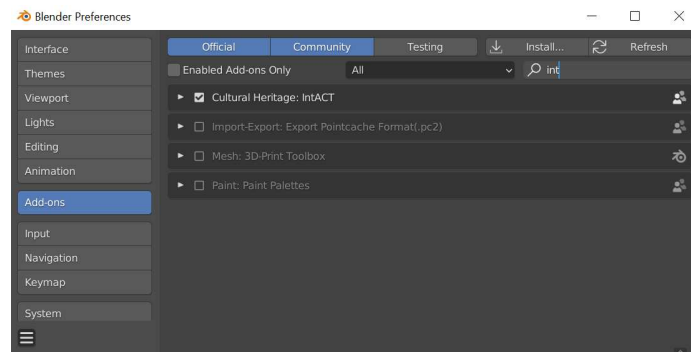


Figure B.3

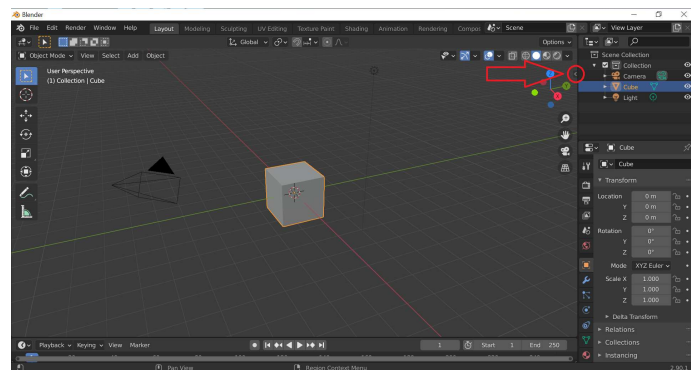


Figure B.4

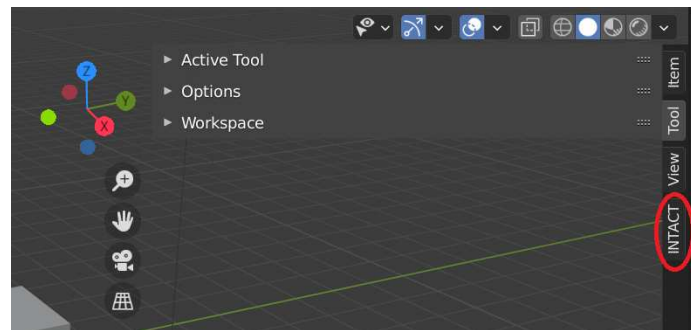


Figure B.5

B.2 The INTACT plugin

The numbering of this section corresponds to the drop-down menu's in the plugin's User Interface (figure B.6).

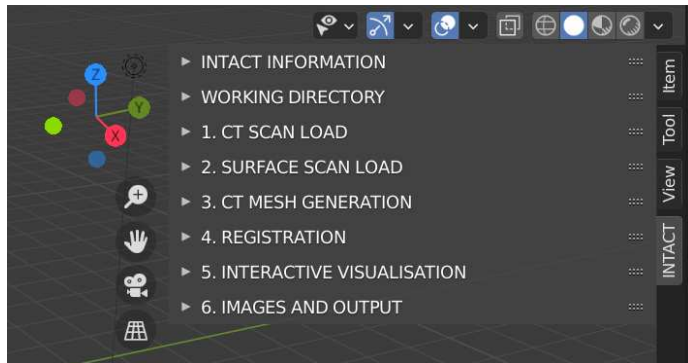


Figure B.6

B.2.0 Setting up working directory

Note: An example dataset is made available to follow along with the guidelines. This includes a 3D-surface scan and a CT scan of a small wooden block. Download the example dataset here: [10.5281/zenodo.8041816](https://doi.org/10.5281/zenodo.8041816)

1. Open INTACT, make it bigger by dragging the side. In the 'Working Directory' tab choose a project directory by clicking on the folder next to the empty field. Make this an empty folder, this is where all the files generated by the plugin will be saved.

B.2.1 Loading CT scan

1. Open the 'CT scan load' tab.
2. Choose a data type (default is Tiff).
3. Input the directory where your CT scan files are stored.
4. In case of Tiff, input the resolution (test dataset voxel size = 0.13mm).
5. Click "Load CT Scan", wait (may take a couple minutes)
6. You can move the view by holding the middle button while moving your mouse. Preferably don't move the CT scan. Don't worry if you do, its position can be reset in the 'CT Mesh Generation' tab.
7. For visualisation purposes you can change the threshold, and color + lighting (figure B.7)

Note: If you do not have a surface scan of your object, you can skip to Visualisation (section B.2.5).

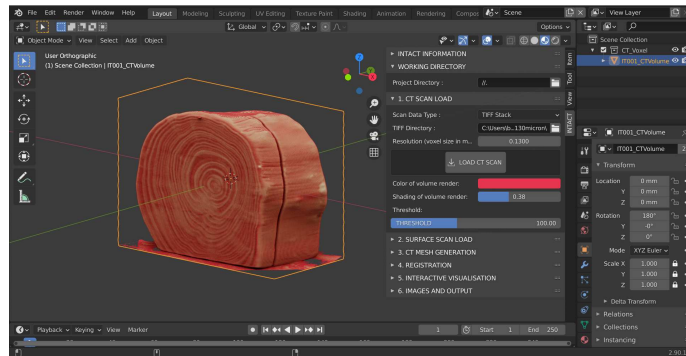


Figure B.7

B.2.2 Surface scan load

1. In the ‘Surface scan load’ tab click on the icon of a folder.
2. In the resulting pop-up, navigate to the directory which holds your 3D model, select the .obj model and click accept. Then click the ‘Load surface scan’ button. (figure B.8).

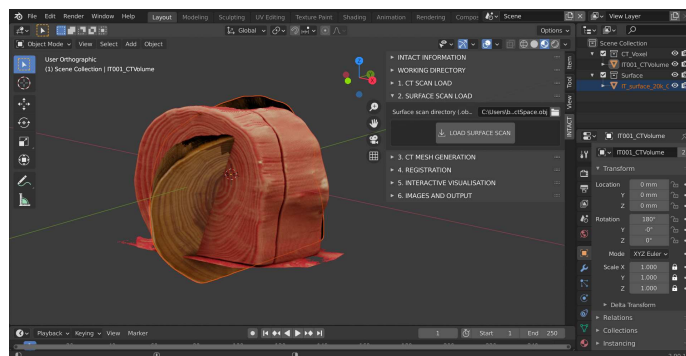


Figure B.8

Tip: Sometimes the surface scan is not shown as expected. This can have to do with how the ‘normals’ are defined. Try going into right hand lower menu, the red ball and change how the normals are calculated. See figure B.9.

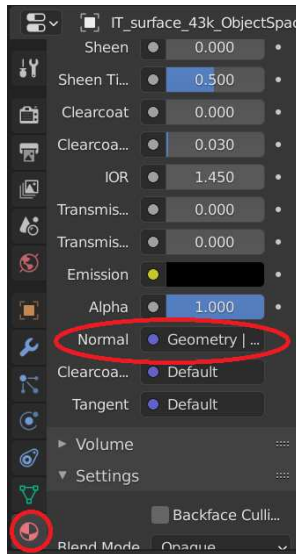


Figure B.9

B.2.3 CT mesh generation

1. In the ‘CT Mesh Generation’ tab, play around with the threshold value to find a value that shows all of the object outline, but not much else. A little noise outside the object is fine.
2. When you’re happy with the threshold, click Segmentation. You’ll end up with a mesh of the CT scan (figure B.10). Wait, this may take a minute. For ease in the next section, it may be nice to turn off the CT volume view by clicking on the eye in the right hand panel, next to the IT001_CTVolume.

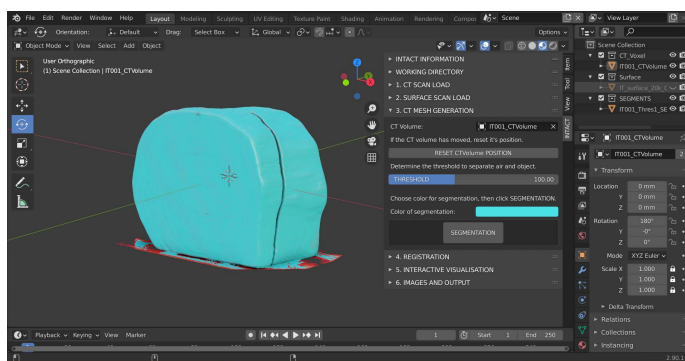


Figure B.10

B.2.4 Registration

1. Select CT scan and if needed because the CT scan was moved, click ‘reset CT volume position’ in the ‘CT Mesh Generation’ tab. Double check that all values are zero (location, rotation) in the lower right panel, the orange square tab will give you these numbers. If not, change them to zero. Scale is 1.
2. Go to the Registration tab.
3. Manually align your 3D surface scan roughly to the produced CT segment, using the controls as described in section 3.3. This can be a rough alignment (figure B.11).
Tip: Use the pre-defined Front/Back – Left/Right – Top/Bottom views, the coloured axis in the top right corner. Switch between those to align your objects manually along each axis.
4. Check that the surface scan and CT segmentation have been identified correctly in the dropdown box and if not select the right objects by clicking the corresponding white eyedropper icon, then clicking the scan/segmentation in the 3D viewer or in the right hand side panel (segmentation is IT001_Thres1_SEGMENTATION). Check “Allow scaling” if you want the surface scan to be scaled if needed.
5. Press ‘Perform Registration’. Wait, this may take a while. You will see a live update of the surface scan mesh move towards the CT mesh (figure B.12).
6. Is the result satisfactory? If it isn’t aligned properly yet, run it again (click the ‘Perform Registration’ button).
 - (a) It won’t align properly? Perhaps your rough manual alignment can be improved. You can also increase the “Outlier %” to 10 or even higher and the iterations can be increased. Experiment a little bit.
 - (b) Look at some landmarks in your object.
 - (c) You should see bits of the CT mesh colour coming through the surface scan.
7. Select your surface scan to see the values for the transformation in the lower right hand panel, orange square tab.

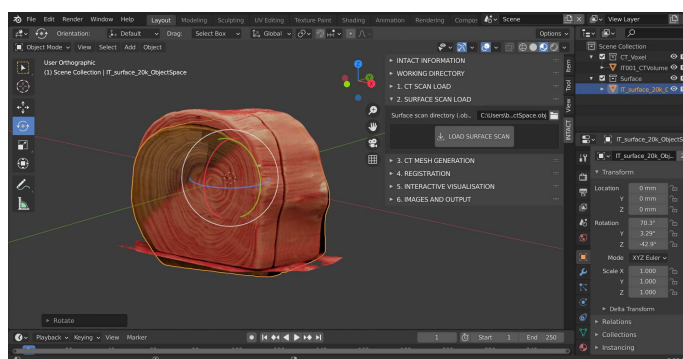


Figure B.11

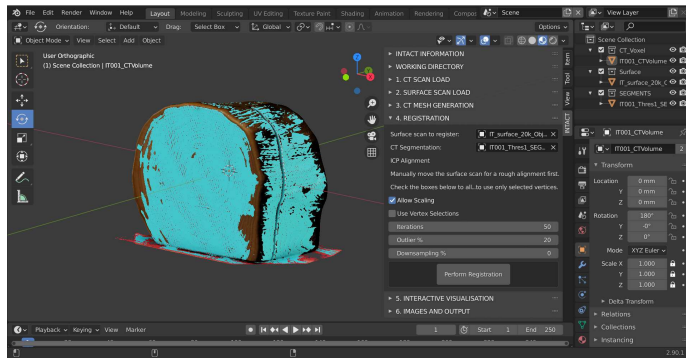


Figure B.12

B.2.5 Interactive visualisation

1. It is usually convenient to hide the visibility of the Segmentation by clicking the eye symbol next to the Segmentation in the right hand upper menu.
2. If given, check the selected CT scan volume, segmentation and surface scan at the top of the ‘Interactive visualisation’ tab. If not, please select them from the dropdown menu, or with the white eyedropper icon as previously described.
3. Then click ‘Slice volume’, to create the CT slices (Figs. B.13 and B.14).
4. If required, adjust the contrast of the slices with the min and max sliders (figure B.15).
5. Click 1Create cropping cube’. This will create a cube, that when moved into the object will make everything within it transparent (figure B.16).
6. Check ‘Track slices’, to attach the slices to the sides of the cube and make them update when the cube is moved into the object.
7. Check ‘Crop slices outside object’ to show only the part of the CT Volume that is inside the object (and not the air around it) (figure B.16).
8. *Optional:* The ‘Multi-view’ button opens up a user interface that shows the X, Y, Z views plus the 3D view.
9. *Optional:* Surface scan roughness and slice thickness can be adjusted.

Now that everything is setup, it is possible to interactively manipulate the data, analyse and investigate. Use the visibilities in the upper right-hand menu and standard Blender controls to move (see section B.3).

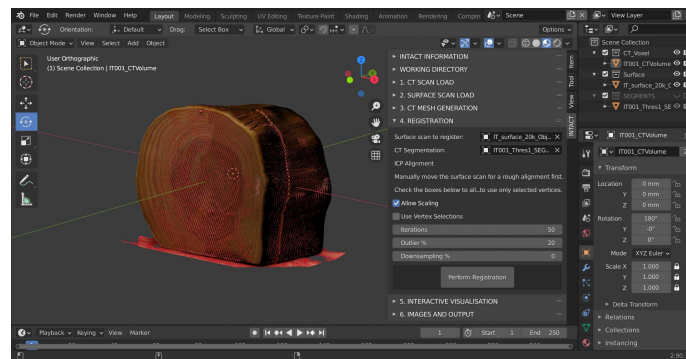


Figure B.13

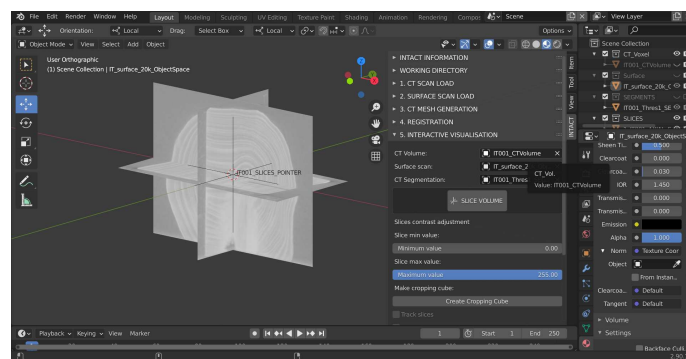


Figure B.14

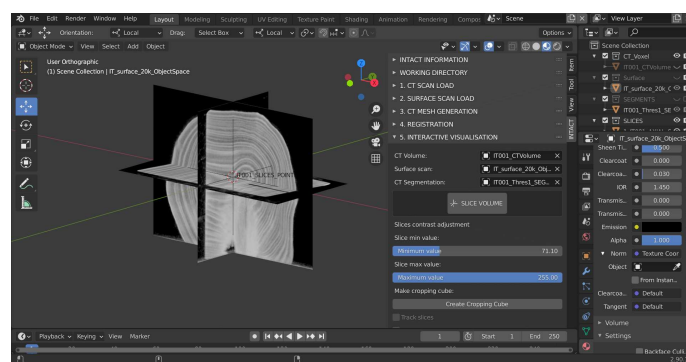


Figure B.15

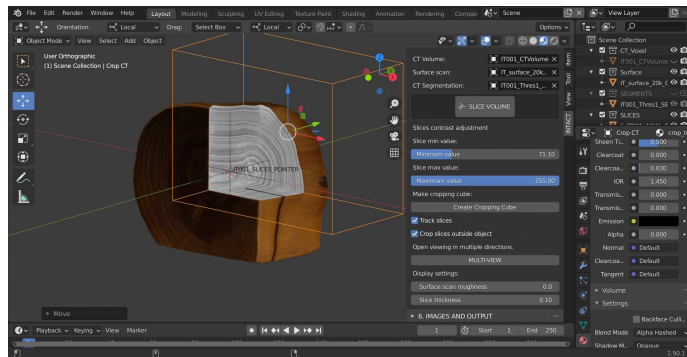


Figure B.16

B.2.6 Images and output

Screenshot:

1. To obtain a screenshot of the current view, including all lines and grids, click ‘Take screenshot’.

Rendering images:

1. Click ‘Set camera position’. This opens up the camera view in a grey rectangle (figure B.17).
2. Change the view of the camera, by moving around using the normal blender controls.
3. Change the size of the camera by changing the resolution parameters.
4. When satisfied click ‘confirm camera position’.
5. *Optional:* Adjust lighting and background colour for the image.
6. Click ‘Render image’. When satisfied, click ‘Image -> Save as...’

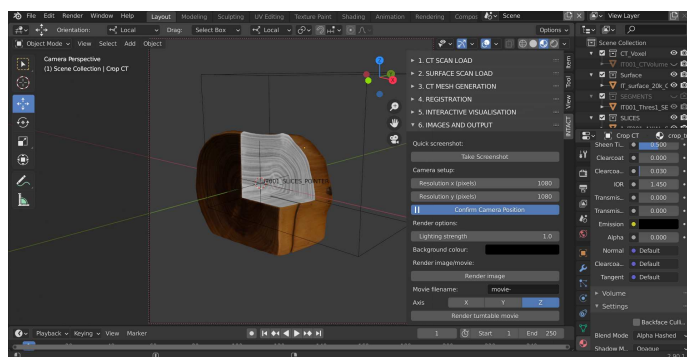


Figure B.17

Rendering videos:

1. The same camera position is used as for the image. If needed, adjust using step 1-4 of Rendering images above.
2. Choose an axis around which to rotate the object.
3. Name the movie - make sure to change this for every movie or the previous one will be overwritten.
4. Click ‘Render turntable movie’. Each frame will be rendered separately and then saved in the working directory in a new folder called ‘Movies’.

B.3 Basic Blender controls

B.3.1 Viewport shading options

The virtual space in which we place our 3D models and objects is called the viewport. There are 4 different shading options within Blender that we can choose from, each with a different appearance (Figs. B.18 and B.19).

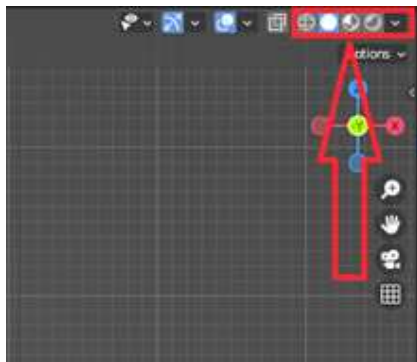


Figure B.18

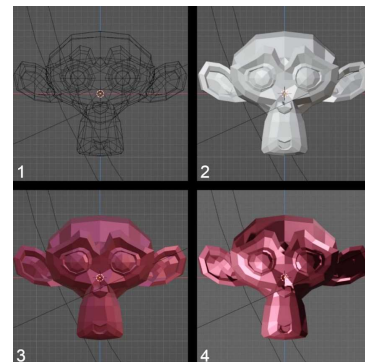


Figure B.19

1. Wire edges

This mode is probably least interesting for our case, and displays the 3D-model as a wireframe.

2. Solid mode

This is the standard mode upon opening blender, and displays the 3D-model as a solid object without its material properties. This mode is best when editing properties, aligning models, or setting up an animation as it's least computationally heavy.

3. Material preview mode

In this mode the material properties are added to the object, as they would appear with relatively flat lighting (not the lights you can add yourself, but what is called ‘world lighting’).

4. Render preview

In this mode the user's 'scene lights' are added. This makes it the most computationally heavy mode as the software has to calculate and render light, reflection, and shadow.

B.3.2 Moving the view

1. Translation

Move the view by holding shift and the middle mouse button, and moving your mouse.

2. Rotation

Rotate the view by holding the middle mouse button, and moving your mouse.

3. Zoom

Zoom in and out by scrolling (either using your trackpad or the middle mouse button).

4. Front-Back-Top-Bottom-Left-Right view

Blender also has 6 built in views that are quickly accessible via the gimbal in the top right corner (figure B.20). You can click on each of the 6 dots (representing X, Y, Z in both positive and negative direction), which will bring you immediately to a view along that axis.

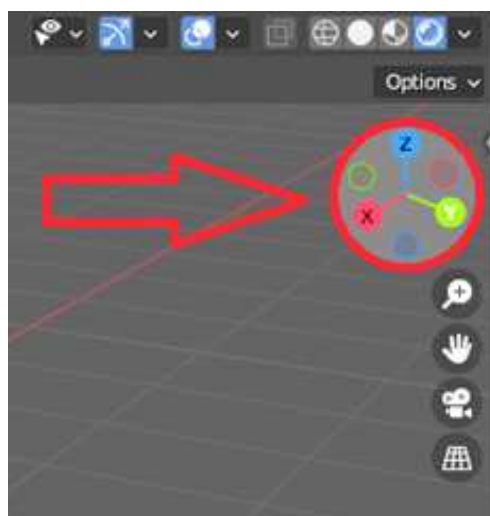


Figure B.20

B.3.3 Object selection/translation/rotation/scaling

1. Select an object

Selecting an object can be done with your left mouse button. You'll see what object is selected in the top right of your screen, in what's called the "Scene collection" (figure B.21A).

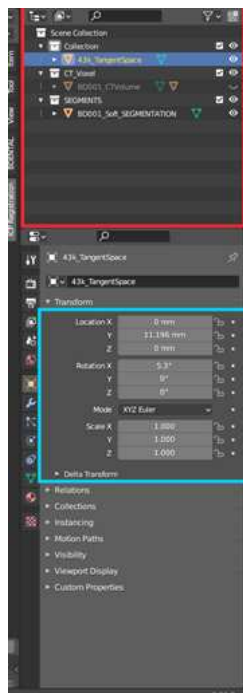
2. Translation/rotation/scaling

There are two ways to move/rotate/scale your object:

- Via the properties panel (figure B.21B) You can change the values in your object's properties panel. This is best for if you want some very subtle changes (e.g. 0.01°).
- In the viewport Click your object, and on the left-hand side you can click "move" and "rotate" (figure B.22). In the centre of your object, handles will appear that allow you to perform these actions along a certain axis, or along all of them at once.

3. Turn on/off visibility and rendering of objects

You might want to enable/disable the visibility of certain objects in your viewport at a given point of time. You can do this by clicking the eye symbol beside the name of your object in the "Scene collection". Clicking the camera will turn on/off the visibility of that object in the rendered image (figure B.23).



A

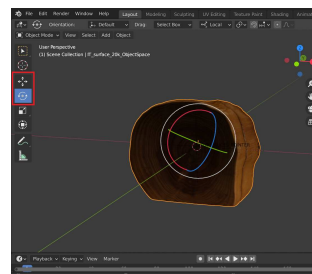


Figure B.22

B

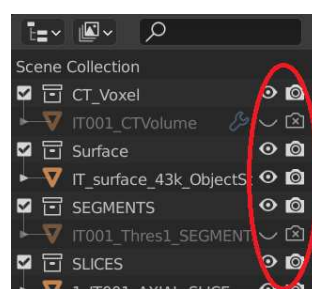


Figure B.23

Figure B.21

B.4 Using vertex selections for registration

B.4.1 Enabling vertex selections

In cases where your X-ray CT or surface scan is incomplete, you may want to focus your registration on a sub-region for the best accuracy. This can be done by enabling the ‘Use Vertex Selections’ option in the Registration tab of the plugin (B.24). You will need to manually select which vertices to include from both your surface scan and CT segmentation mesh. Only choose areas that appear in both for the best accuracy.

B.4.2 How to select vertices

1. To select vertices, you have to enter Blender’s ‘Edit mode’. First select the mesh you want to use, then change the dropdown menu in the top left of the viewport to edit mode (figure B.25). Alternatively, you can select the mesh, and press the tab key on your keyboard. To go back to the normal blender mode, change the menu to ‘Object Mode’, or press tab again.
2. Once in edit mode, you can select vertices by clicking and dragging across the parts of the mesh you want to include (figure B.26). Selected vertices will appear in bright orange. To add to your selection, hold down the shift key while you do this.
3. To select through your mesh (i.e. not just vertices on the face closest to you), you can enable Blender’s X-ray mode. Click the symbol with two overlapping squares in the top right of the viewport (figure B.27) or press alt + Z on your keyboard.

B.4.3 Tips for selecting vertices

- In some meshes, you may have multiple regions that aren’t directly connected to each other. To select all vertices in one piece, you can click one vertex, then press ctrl + L to select everything connected to it.
- It can also be useful to hide parts of the mesh you don’t want to select. This can be done by selecting the vertices (in the usual way), and pressing H to hide them. Any hidden vertices can be shown again by pressing alt + H.
- A line of vertices can be selected by clicking a vertex at one end, then ctrl + click a vertex at the other end. Blender will select all vertices on the shortest path between the two.
- Combining these methods can make selecting sub-regions much faster. For example, you could select a line of vertices that separate your region of interest from the rest of the mesh. Hiding this will disconnect your region of interest, and allow it to be selected in one go with ctrl + L.

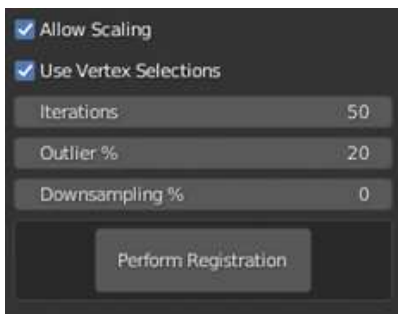


Figure B.24



Figure B.26

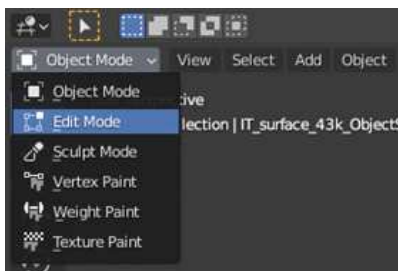


Figure B.25

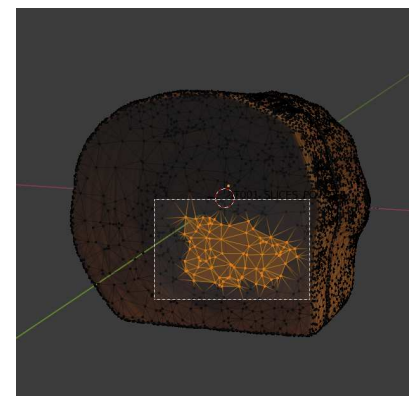


Figure B.27

List of publications

Publications that are part of this thesis:

1. F. G. Bossema, W. J. Palenstijn, A. Heginbotham, M. Corona, T. Van Leeuwen, R. Van Liere, J. Dorscheid, D. O'Flynn, J. Dyer, E. Hermens, and K. J. Batenburg. "Enabling 3D CT-scanning of cultural heritage objects using only in-house 2D X-ray equipment in museums". *Nature Communications* (accepted, in press).
2. F. G. Bossema, P. J. Van Laar, K. Meechan, D. O'Flynn, J. Dyer, T. Van Leeuwen, S. Meijer, E. Hermens, and K. J. Batenburg. "Inside out: Fusing 3D imaging modalities for the internal and external investigation of multi-material museum objects". *Digital Applications in Archaeology and Cultural Heritage* 31 (2023), e00296.
3. F. G. Bossema, M. Domínguez-Delmás, W. J. Palenstijn, A. Kostenko, J. Dorscheid, S. B. Coban, E. Hermens, and K. J. Batenburg. "A novel method for dendrochronology of large historical wooden objects using line trajectory X-ray tomography". *Scientific Reports* 11, 11024 (2021).
4. F. G. Bossema, S. B. Coban, A. Kostenko, P. van Duin, J. Dorscheid, I. Garachon, E. Hermens, R. van Liere, and K. J. Batenburg. "Integrating expert feedback on the spot in a time-efficient explorative CT scanning workflow for cultural heritage objects". *Journal of Cultural Heritage* 49 (2021), pp. 38–47.

Publications that are not part of this thesis:

1. M. Domínguez-Delmás, P. Van Duin, J. Dorscheid, F. G. Bossema, K. J. Batenburg, and R. Van Langh. "Unravelling a 17th-century prison escape: The quest to identify the original Hugo Grotius bookchest". In: *Working Towards a Sustainable Past*. ICOM-CC 20th Triennial Conference Preprints, Valencia, 18–22 September 2023, J. Bridgland. Paris: International Council of Museums, 2023
2. F. Bossema, C. Zwetsloot, and I. Smeets. "Math in the City: Designing a Math Trail for High School Students". In: *World Scientific Series on Science Communication*. Vol. 03. WORLD SCIENTIFIC, 2023, pp. 53–72.
3. M. Kiss, F. G. Bossema, P. J. Van Laar, S. Meijer, F. Lucka, T. Van Leeuwen, and K. J. Batenburg. "Beam filtration for object-tailored X-ray CT of multi-material cultural heritage objects". *Heritage Science* 11, 130 (2023).
4. J. Dorscheid, F. G. Bossema, P. van Duin, S. B. Coban, R. van Liere, K. J. Batenburg, and G. P. Di Stefano. "Looking under the skin: multi-scale CT scanning of a peculiarly constructed cornett in the Rijksmuseum". *Heritage Science* 10, 161.1 (2022).

5. M. Domínguez-Delmás, F. G. Bossema, J. Dorscheid, M. Hall-Aquitania, S. B. Coban, K. J. Batenburg, and E. Hermens. “X-ray computed tomography for non-invasive dendrochronology reveals concealed double paneling on a painting from Rubens’ studio”. *PLOS ONE* (2021).
6. M. Domínguez-Delmás, F. G. Bossema, B. van der Mark, A. Kostenko, S. B. Coban, S. van Daalen, P. van Duin, and K. J. Batenburg. “Dating and provenancing the Woman with lantern sculpture – A contribution towards attribution of Netherlandish art”. *Journal of Cultural Heritage* 50 (2021), pp. 179–187.
7. F. G. Bossema, P. Burger, L. Bratton, A. Challenger, R. C. Adams, P. Sumner, J. Schat, M. E. Numans, and I. Smeets. “Expert quotes and exaggeration in health news: a retrospective quantitative content analysis”. *Wellcome Open Research* 4 (2019), p. 56.
8. J. Schat, F. Bossema, M. E. Numans, I. Smeets, and P. Burger. “Overdreven gezondheidsnieuws: Relatie tussen overdrijving in academische persberichten en in nieuwsmedia”. *Nederlands Tijdschrift voor Geneeskunde* (2018).
9. F. Bossema, J. Retrê, S. Pereira, and P. Russo. “Your night out under the stars: Reaching beyond native audiences”. *Communicating Astronomy with the Public* (2018).

Published datasets and code related to this thesis:

1. F. Bossema. *Radiographic data of a wooden block with metal markers at the FleX-ray laboratory (high resolution)*. 2024. URL: <https://zenodo.org/records/10557034> (visited on Mar. 19, 2024)
2. F. Bossema, A. Heginbotham, and M. Corona. *Radiographic data of 'Python killing a Gnu' by Antoine-Louis Barye, The J. Paul Getty Museum collection*. 2024. URL: <https://zenodo.org/records/8379913> (visited on Mar. 19, 2024)
3. F. Bossema and D. O'Flynn. *Radiographic data of a wooden block with metal markers at the British Museum X-ray facility*. 2024. URL: <https://zenodo.org/records/8379910> (visited on Mar. 19, 2024)
4. F. Bossema and A. Heginbotham. *Radiographic data of a wooden block with metal markers at the J. Paul Getty Museum X-ray facility*. 2024. URL: <https://zenodo.org/records/8379880> (visited on Mar. 19, 2024)
5. F. Bossema. *Radiographic data of a wooden block with metal markers at the Rijksmuseum X-ray facility*. 2024. URL: <https://zenodo.org/records/8379870> (visited on Mar. 19, 2024)
6. F. Bossema. *Code for 3D tomography using only basic X-ray equipment and metal markers*. 2024. URL: <https://zenodo.org/records/8379920> (visited on Mar. 19, 2024)

7. F. Bossema and P. Van Laar. *CT reconstruction and structured light scan of a small wooden block*. 2023. URL: <https://zenodo.org/records/8041816> (visited on Nov. 9, 2023)
8. F. Bossema, P. Van Laar, and K. Meechan. *IntACT plugin for Blender*. 2023. URL: <https://zenodo.org/records/8041844> (visited on Nov. 9, 2023)
9. F. G. Bossema. *A CT dataset of a small wooden block*. 2021. URL: <https://zenodo.org/record/4533882> (visited on Nov. 9, 2023)
10. F. G. Bossema. *A line trajectory X-ray tomography dataset of a wooden plank*. 2021. URL: <https://zenodo.org/record/4533887> (visited on Nov. 9, 2023)
11. F. G. Bossema, J. Dorscheid, A. Kostenko, and S. B. Coban. *A line trajectory X-ray tomography dataset of the Hugo de Groot bookchest*. 2021. URL: <https://zenodo.org/record/4533923> (visited on Nov. 9, 2023)
12. F. G. Bossema. *Three line trajectory X-ray tomography datasets of a small wooden block*. 2021. URL: <https://zenodo.org/record/4541555> (visited on Nov. 9, 2023)
13. F. G. Bossema and S. B. Coban. *Three tomographic CT datasets of a woven fabric*. 2020. URL: <https://zenodo.org/records/3741311> (visited on Nov. 9, 2023)
14. F. G. Bossema, A. Kostenko, and S. B. Coban. *A five-tile tomographic micro-CT dataset of the oak sculpture "Holy woman with lantern" - part 1 of 2*. 2020. URL: <https://zenodo.org/record/3747192> (visited on Nov. 9, 2023)
15. F. G. Bossema, A. Kostenko, and S. B. Coban. *A five-tile tomographic micro-CT dataset of the oak sculpture "Holy woman with lantern" - part 2 of 2*. 2020. URL: <https://zenodo.org/record/3747327> (visited on Nov. 9, 2023)

